Geomechanics for Energy and the Environment 24 (2020) 100169

Contents lists available at ScienceDirect

Geomechanics for Energy and the Environment

journal homepage: www.elsevier.com/locate/gete

Laboratory simulations of fluid-induced seismicity, hydraulic fracture, and fluid flow

Philip M. Benson [a,*], David Carlo Austria [a,b,**], Stephan Gehne [a], Emily Butcher [a], Claire E. Harnett [c], Marco Fazio [d], Pete Rowley [e], Ricardo Tomas [a]

[a] Rock Mechanics Laboratory, School of Earth and Environmental Sciences, University of Portsmouth, PO1 3QL, UK
[b] Geosciences and Reservoir Engineering Group, Energy Development Corporation, Ortigas Centre, Pasig City, Philippines
[c] School of Earth Sciences, University College Dublin, Dublin, Ireland
[d] Geowissenschaftliches Zentrum, Universität Göttingen, Angewandte Geologie Goldschmidtstrasse 3, 37077, Göttingen, Germany
[e] Department of Geography and Environmental Management, University of the West of England, Frenchay campus, Bristol, BS16 1QY, UK

ARTICLE INFO

Article history:
Received 28 May 2019
Received in revised form 16 December 2019
Accepted 17 December 2019
Available online 20 December 2019

Keywords:
Fluid-induced seismicity
Acoustic emission
Hydraulic fracture
Geomechanics

ABSTRACT

Fluid-induced seismicity has been observed and recorded for decades. Seismic energy necessarily requires a source, which is frequently related to rock fracture either in compression or tension. In both cases, such fracture may be promoted by crustal fluids. In this paper, we review some of the advances in the field of fluid-induced seismicity, with a particular focus on the use and application of new and innovative laboratory methods to better understand the complex, coupled, processes in shallow sub-surface energy extraction applications. We discuss the current state-of-the-art with specific reference to Thermal-Hydraulic-Coupling in volcanotectonic environments, which has a long history of fluid-driven seismic events linked to deep fluid movement. This ranges from local earthquakes to fluid-driven resonance, known as volcanic tremor. More recently so-called non-volcanic tremor has been identified in a range of scenarios where motion at an interface is primarily driven by fluids rather than significant stress release. Finally, we review rock fracture in the tensile regime which occurs naturally and in the engineered environment for developing fractures for the purpose of resource extraction, such as hydraulic fracturing in unconventional hydrocarbon industry or developing Hot-Dry-Rock geothermal reservoirs.

1. Introduction

Fluids in the crust are ubiquitous, generally following a hydrostatic pressure increase with depth as long as the host rock mass is sufficiently porous and permeable to allow free movement of fluids (e.g. Refs. 1, 2). Such a relationship applies to most crustal rocks, with the hydrostatic gradually deviating to the lithostatic pressure gradient over a depth range spanning 4 to 6 km. Below 8 km, most crustal rocks have insufficient connected porosity for significant permeability and so pore pressure is essentially the same as lithostatic pressure (e.g. Ref. 3; Ref. 4). Consequently, pore pressures at depth, when trapped in low permeability country rocks, give rise to natural hydraulic fracturing and are seen in a range of environments resulting in features such as veining and mineralization.[5,6] In addition, elevated temperatures may drive more exotic styles of fluid-driven fracture via dehydration and friction on faults, which locally increase pore fluid pressure (e.g. Refs. 7–9) to fracture rocks in tension, their weakest failure mode (e.g. Refs. 1, 4).

At shallower levels (0–2 km), fluid-driven fracture is seen in a range of environments. In volcanic areas the combination of high geothermal gradient, geothermal and magmatic fluids, and an often complex hydrogeological system provides evidence for tensile fracture in magmatic bodies.[10,11] There is evidence that a diverse range of seismo-tectonic activity (e.g. Chouet et al., 1996) accompanies these processes. This covers brittle (tensile) failure, known as volcano-tectonic (VT) events, to characteristic seismic signals resulting from resonance within the pressurized fluid, likened to the 'tone' generated from an organ pipe or resonator[12,13] and known as long-period (LP) tremor. Although still controversial, a number of laboratory studies (e.g. Ref. 14; Fig. 1; Ref. 15) have confirmed the general principle of rock-fluid coupling behind these characteristic signals. For a time, this was thought to be specific to volcanoes, however recent evidence has revealed similar effects at depth (e.g. subduction zones), where fluids lubricating the fault zone and over pressurized fluids reducing the effective normal stress result in a

* Corresponding author.
** Corresponding author at: Geosciences and Reservoir Engineering Group, Energy Development Corporation, Ortigas Centre, Pasig City, Philippines.
E-mail addresses: philip.benson@port.ac.uk (P.M. Benson), austria.ds@energy.com.ph (D.C. Austria).

https://doi.org/10.1016/j.gete.2019.100169

plethora of slip events including similar signals known as non-volcanic tremor (e.g. Refs. 8, 16). In the case of the engineered environment, intentional hydraulic fracturing has now become a common method to extract unconventional oil and gas from otherwise inaccessible and unconnected porosity (e.g. Refs. 17–19). This method, although controversial, has transformed the energy landscape, particularly in the US. However, induced seismicity, primarily generated as the rock mass is fractured in tension and triggering local earthquake swarms, also results from the reactivation of local fault zones. This remains a significant concern (e.g. Refs. 20–25).

Applications combining fluid-driven tensile failure and elevated heat flow, such as the volcano-tectonic areas noted above, also include geothermal energy production. Two forms of reservoirs are generally considered, the conventional "Hot-Wet-Rock" type of reservoir where the porosity of the host rock mass is naturally filled with fluid and engineered geothermal systems (EGS). In the former, extraction requires a simple well, as exploited in Iceland, where this system provides some 700 MW of power. In EGS (also known as "Hot-Dry-Rock") two wells are required: a first well drilled into a rock mass is used to stimulate (fracture) the surrounding country rock, in addition to any natural porosity and permeability, and thus be hydraulically connected to a second well. Fluid is then pumped from one well to a second (or via a network of wells) using the natural heat from the rock mass to increase the temperature of a working fluid for energy extraction. Many areas are suitable for such development, such as mountain ranges (e.g. Italian Alps: Zappone et al[26]) and volcano-tectonic areas (e.g. Long Valley, California: Hildreth[27]). In the Philippines, which produces more than 1.8 GW of electricity from geothermal energy, conventional geothermal systems are combined with hydrofracturing to further improve well permeability and promote more water-rock heat transfer. However, stimulating a rock mass by injecting fluids to create tensile fracture networks to link the wells is not without risk. Unmapped pre-existing fractures, in common with hydrocarbon-driven hydraulic fracture, have frequently given rise to unexpected seismicity due to reactivation of dormant faults, such as reported during the geothermal project in Basel, Switzerland and in other geothermal systems (e.g. Refs. 28–31).

In all these cases, the energy release is often monitored for the purposes of fundamental research, safety and forecasting, as well as to better optimize resource extraction. In the case of geothermal extraction and hydraulic fracking, simple "traffic light" systems are often used which pause operation if seismic events above a threshold are detected and thus to provide a safety control for seismic hazard.[21,28] In geothermal extraction, experience in the Philippines suggests that the number and magnitude of seismic events is generally higher in areas with fluid extraction compared to the fluid injection areas. This is consistent with data from volcano-tectonics both in the field (e.g. Refs. 13, 32, 33) and the laboratory (e.g. Refs. 14, 34) which show that the fluid-rock interaction has a significant control on the radiated energy during pressure release, which is also related to phase changes (water to steam). The use of controlled laboratory experiments is now starting to place better constraints on the triggers (pressure, stress) that result in tensile fracture and shear events, and once a permeable network is generated, yield characteristic seismic signals generated by fluid-rock interaction. Acoustic Emission (AE) has a long history in the field of laboratory rock deformation and rock physics, with early work pioneered by researchers in the late 1970's (e.g. Refs. 35–37). AE is typically described as a high frequency strain wave in the kilohertz to megahertz range, and is now well established as a proxy for field scale seismicity (e.g. Refs. 15, 34, 38–41). Such AE sensors may be operated passively (for 3D hypocentre location) or actively for determination of elastic wave velocities (e.g. Refs. 42, 43).

Importantly, the scaling of AE data follows power law relationships and thus allows similar statistics across these scales to be employed.[44–46] The similarity arises because the probability of fracturing follows the classical Boltzmann statistical distribution at all length scales. It is likely that similar unifying principles will hold for events at different scales. This suggests that the event generation process is governed by crack morphology; under the stress conditions of interest, the crack distribution and morphology is likely to be scale-invariant.[47] Such statistical methods are of crucial importance, as this type of analysis permits laboratory experiments (which we control) to investigate natural processes (which we cannot control) with some level of confidence. Finally, although the majority of experiments have tended to focus on qualitative effects (e.g. Refs. 15, 43, 48), recent data from calibrated AE is now closing the gap between quantified seismic data in the field, and how this links to the seismic source.[49–52]

Understanding these complex coupled processes is therefore difficult, both due to the inherent difficulty in observing the deep-seated processes, as well as the difficulty of rigorously measuring fluid-pressure driven mechanical effects in time and space. Yet, a full understanding of these is needed to optimize energy extraction in hydraulic fracture and geothermal systems, to name just two examples. In this paper, we review some of the methods developed over the last 15 years that apply innovative laboratory methods to simulate the process of hydraulic fracture and fluid-driven tensile mechanics. We then discuss this in the contact of some recently acquired data using andesite taken from the South Negros geothermal field in the Philippines.

2. Methods

To better understand processes in the field, innovative laboratory methods have been widely developed. More recent work has now evolved to a point where a diverse range of parameters are measured simultaneously at very high sampling rates (e.g. fluid pressure, stress, strain), performed in conventional triaxial setups (e.g. Refs. 49, 53), and true-triaxial setups often using cubic specimens (e.g. Refs. 54, 55). In addition, innovative post-test techniques such as X-ray Computed Tomography (CT), and fluorescence of the crack tip are now exploring the details of the fluid-dynamics operating at the crack tip (e.g. Refs. 48, 56, 57). At the elevated temperatures applicable to geothermal extraction (but employing similar tensile fracture mechanics), the extreme conditions pose unique challenges to the experimentalist. Despite these challenges, a small number of laboratory studies have been reported ranging from the use of pressurized semi-molten rock (e.g. Refs. 58, 59), to a lower temperature (and more controllable) proxy such as softened PMMA (polymethyl methacrylate) or wax (e.g. Refs. 60–62). In these cases, the investigation is often more aligned to high temperature dyke injection and dynamics, rather than hydraulic fracturing. However, many authors in the field of volcanology do note that despite the obvious high temperatures involved, the fundamental tensile mechanics are essentially the same as per engineered applications such as fracking (e.g. Ref. 63). Finally, laboratory methods at elevated pressure and temperature include simulations of fundamental fracture mechanics but without using high-pressure fluid, by using short rod specimens (e.g. Refs. 64, 65). However, this type of setup does carry with it the disadvantage that the specimen failure also concludes the experiment, as the short rod sample is no longer sealed.[66]

Importantly, and in common with all the above examples, the use of a well-controlled laboratory methodology has the key advantage of offering a controlled and consistent environment with which to test ideas. And, whilst the smaller scale samples are often cited as a weakness, the ability to quickly investigate the changing material properties and the effects on external stimuli

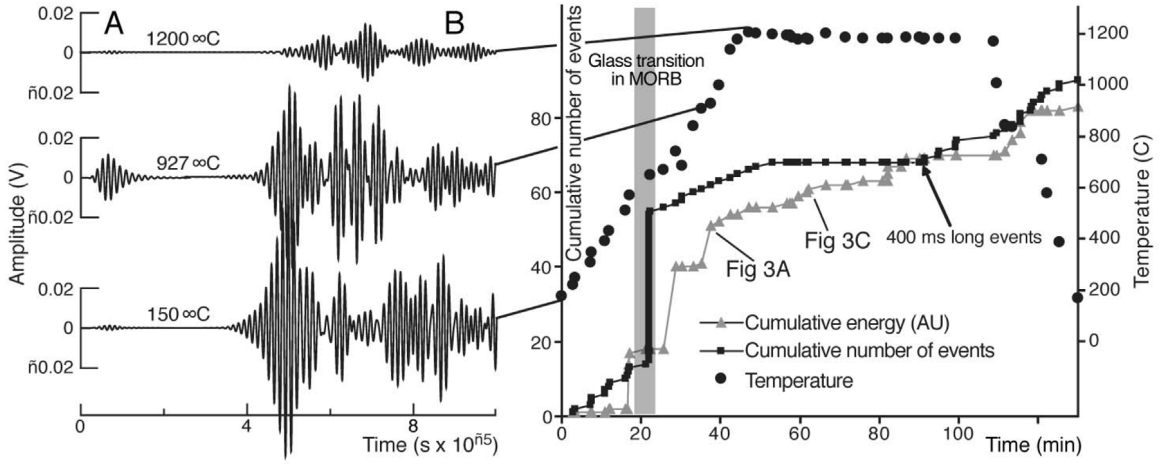

Fig. 1. Example of laboratory seismicity (known as Acoustic Emission) generated during high temperature simulations of melting in Mid Ocean Ridge Basalt (MORB). As fluid migrates, characteristic "Low Frequency events are preferentially generated, with the number of events (black line) accelerating dramatically as the temperate increases through the glass transition. After Ref. 14.

(stress, pressures and temperatures) on the sample allows for a powerful *holistic* rock physics interpretation to be formulated. And, although the true stress state in the Earth is best described as "true triaxial" whereby $\sigma_1 > \sigma_2 > \sigma_3$, the complexity and expense of designing, fabricating, and operating such apparatus with cubic specimens (e.g. Refs. 55, 57) has led to researchers opting for the so-called "conventional" triaxial cell (e.g. Refs. 34, 49, 67, 68). By modifying these apparatus (Fig. 2) to replace the sample assembly for different fluid-injection scenarios, a number of physical properties may be measured, including Acoustic Emission (Fig. 2A). A typical setup is of a cylindrical core (15–50 mm diameter and up to 125 mm length, typically with a length: diameter ratio of between 2 and 2.5 and with ends ground flat to a precision of 0.01 mm) encapsulated in a rubber jacket to isolate the sample from the confining pressure medium. To investigate fluids within the damage zone a sample drilled with a thin axial conduit (Fig. 2B), has been developed (e.g. Ref. 15; Benson et al., 2011). In these experiments, reported by Fazio et al.[34,69]), a water saturated 40 mm diameter sample (100 mm long) drilled with a 3 mm conduit was first deformed at 35 MPa confining pressure to generate a shear fault. After returning to the initial conditions (35 MPa confining pressure and 5 MPa pore pressure), the high-pressure pore fluid (water) is released to atmosphere to promote fluid-decompression generated turbulence in the damage zone analysing these fluid-mechanical effects with an array of AE sensors.[15]

To understand fracture in tension, the use of so-called thick-walled cylinder tests has an extensive literature with early work concentrating on the mechanical effects and developing models of the process.[70–72] In low permeability rock such as shale and granite (crystalline rock), designing an apparatus to fracture a shale in tension due to fluid overpressure is relatively simple (e.g. Fig. 2C). Conversely, using a rock of higher porosity (and hence permeability) needs some form of rubber 'liner' inside the inner bore (e.g. Ref. 67) to allow the stress to build at the inner wall of the setup. Without this, a simple shear fracture will develop, promoted by the decrease of the effective pressure ($p_{eff} = p_c - p_p$) as fluid is injected (e.g. Ref. 68). Newer approaches now combine these fluid-mechanical methods with AE recorders to better understand the developing fracture (e.g. Refs. 57, 68, 73). The laboratory setup described by Gehne et al,[53] is a variation of this, but further modified to additionally measure very-high speed mechanical data (stress, strain, pore pressure) as well as the permeability[74] by using the high speed data recorders for AE as a digitization tool for stress, strain, and pressure data (Fig. 2A; Gehne et al.[53]).

In some apparatus, an integrated furnace allows the setup to be heated, with the maximum achievable temperature usually dependent on the type of furnace used. For external furnaces, typically wrapped around the pressure vessel in 'clam-shell' or printed form, this is typically around 200 °C (e.g. Refs. 34, 69). Furnaces that are internal to the pressure vessel, usually utilizing Argon gas for the confining pressure medium rather than silicone oil to avoid polymerization effects at high temperature and pressure, reach up to 1200 °C. Of the designs, the most ubiquitous is the "Paterson" apparatus, after its inventor.[4] These allow a wide range of investigations including High-Pressure/High-Temperature elastic wave velocity measurements (Zappone and Benson, 2011; Fig. 3), fluid-driven seismicity (Refs. 14, 75; Fig. 1), phase changes (e.g. Refs. 7, 76) in addition to triaxial rock deformation (e.g. Ref. 77).

The two setups (Fig. 2B, C), in conjunction with high speed recording systems (Fig. 2A), allow a wide range of rock deformation (shear and tensile) studies to be performed, monitored via a suite of rock physics methods. Of these, three methods are common. *Firstly*, elastic wave velocity data (P-wave and S-wave) are generated by pulsing each of the AE sensors in sequence, with the remaining sensors receiving the waveform. Output waveform data (voltages) are received by a preamplifier and boosted by (typically) 20–60 dB according to received amplitude. By referring to the known positions of the sensors, elastic wave velocity is derived via the time-of-flight method of Birch.[78] *Secondly*, the AE data may be used to locate the source of fracturing in 3D due to deformation (e.g. Refs. 37, 41, 79) by recording the full waveform received at each sensor and recording the onset time at each channel. Inversion for 3D hypocentre location may then be made based on the measured velocity model. The AE recording systems have evolved over the last 20 years from systems that simply digitize the discrete waveforms once a trigger criterion (typically when any single channel observes an AE event above a target threshold of approximately 5× noise level, or approximately 100 mV) had been met (e.g. Ref. 37), to continuous AE systems that continuously digitize the voltage to storage for later offline processing (e.g. Refs. 41, 68, 80). The later systems have the advantage of not missing any information during the time needed for the processors to record and then 're-arm' for the next event. Both types of recorder typically digitize the data at a sampling rate of 10 MHz at 16-bit resolution.

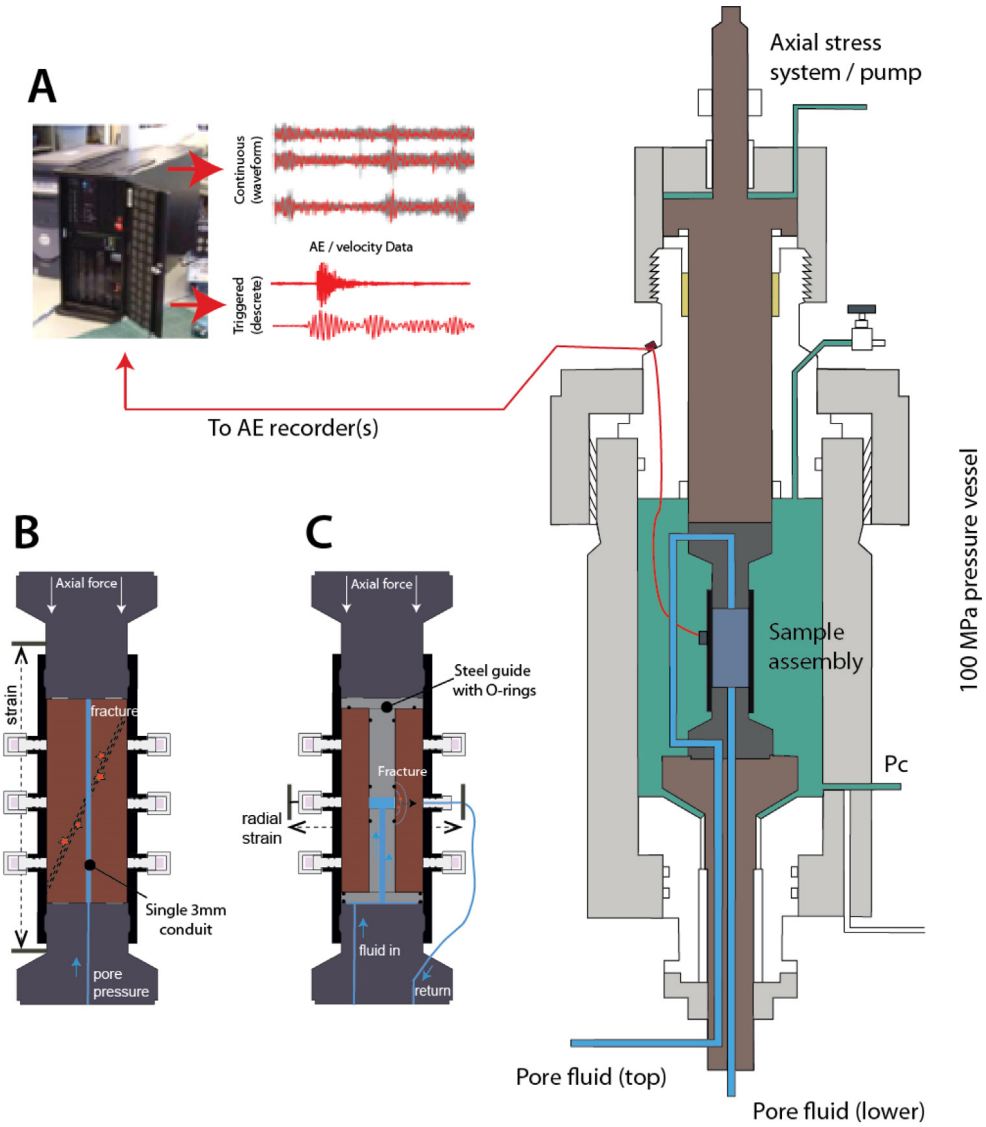

Fig. 2. Typical laboratory triaxial deformation apparatus (panel A) and sample assemblies for standard deformation with a shear-fault (panel B), and fluid-driven tensile fracture (panel C). In all cases a network of Acoustic Emission (AE) sensors records the generated micro-seismic activity for comparison to mechanical and fluid pressure data.
Source: Modified from Refs. 34, 53.

If fluids are present, further experiments may then be made of the fluid flow through those damage zones, akin to the rock-fluid-turbulence driven volcanic tremor introduced earlier. Whilst hypocentre locations of the fluid-driven stage have been reported (e.g. Ref. 15; Benson et al., 2011) the emergent nature of the waveform and the generally lower energy of these events result in fewer locations compared to compressional/shear fracture. As an alternative, a simple 'hit rate' – defined as the number of times a channel exceeds a threshold voltage in a short time window – may be calculated. Although basic, this method is still useful for defining the rate of change of fracturing during very high-speed events, such as during tensile fracture, without recourse to exotic means to slow down the deformation such as AE feedback (e.g. Ref. 37). *Thirdly*, mechanical data consisting of axial and radial deformation is collected using sensors such as linear variable displacement transducers (LVDT's), load cells and pressure sensors, and across a range of sampling rates appropriate to the process under test and suitable signal conditioning. Axial deformation is used as a servo control feedback loop to control the sample deformation (where used), at typical strain rates between of 1×10^{-5} s^{-1} to 1×10^{-5} s^{-1}. To understand high pore fluid pressure changes during hydraulic fracture of samples or during the venting of water, data in recent studies[34,53] is sampled at low (1 Hz), high (10 kHz), and very high (10 MHz) rates. Taken together, these three methods permit a full 'rock physics' profile of the deforming system – either compression or tensile – to be recorded for later processing.

3. Typical data generated from modified triaxial assembles and "rock physics ensembles"

The methods above have been widely reported in the rock deformation and rock physics literature, and although the reproduction of the precise conditions is not always feasible, the use of holistic approaches have greatly elucidated how changes in recorded parameters occur due to the imposed (measured) conditions simulating deep geophysical processes. To reinforce this, we present below three examples of recently published data across the three methods reviewed above.

(i) Elastic wave data: mineral effects and fracture damage zones.
It is well known that elastic wave velocities are very sensitive to changes in mineral composition, phases, and fracture and crack

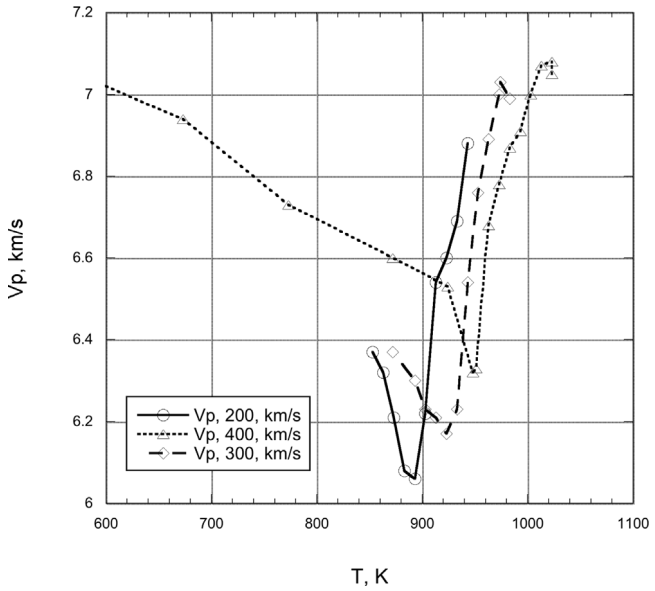

Fig. 3. Evolution of P-wave elastic velocity from a quartz-rich metapelite from Northern Italy. For each of the three confining pressures tested (200 MPa: solid line; 300 MPa, dashed line; 400 MPa, dotted line) the P-wave velocity decreases before recovering at 890, 920 and 950 K respectively. This pressure dependent inflexion mirrors the alpha–beta phase change in the quartz. After Zappone and Benson, 2011.

damage of a rock mass (e.g. Refs. 42, 67, 81). This is due to a range of factors such as energy partitioning, reflection, and scattering/attenuation effects (e.g. Ref. 82). For this reason, it is important to both understand the effects that fracturing has on the seismic propagation in the material, often used for seismic tomography imaging of structures (e.g. Refs. 83, 84), and also to better understand the seismic source from measured surface data (e.g. Refs. 76, 85). Increasing temperature also has an effect, both from thermal stressing effects from differential expansion of mineral phases leading to grain boundary cracking lowering elastic wave velocity (e.g. Refs. 83, 86–88) but also due to phase changes, likely to be especially important in geothermal areas (e.g. Fig. 3; Zappone and Benson[26]). In addition, the directional dependence of the elastic wave velocity may be used to infer the orientation of a damage plane if sufficient data is available.[89,90] Fig. 4 shows this effect using data from three volcanic rocks from the volcanic islands of El Hierro and Tenerife (Canary Islands, Spain) and Stromboli (Aeolian Islands, Italy) with initial porosities of 1.7%, 12.3% and 6.1% respectively[89] where the normalized elastic wave velocity (P-wave) is tracked during fracture development across a range of incident angles relative to the shear fault plane (measured via post-test examination).

Using these rocks and the triaxial apparatus described above (Fig. 2A and B) with a dry sample, and a strain rate of 10^{-5} s^{-1} to generate a shear fault due to compression, it is evident that the formation of the fault has a dramatic effect on the evolution of elastic wave velocity. In each case, as the experiments progress, elastic-wave velocity first increases, reaching a maximum as pre-existing cracks close. Cracks then reopen, finally coalescing into a shear fault when a significant decrease in P-wave elastic velocity is seen (e.g. Ref. 91).

In addition to this overall trend, the normalized velocity decrease is strongly dependent on the angle of the raypath with respect to the shear plane as verified from post-mortem analysis (Fig. 4). In samples with a low initial porosity (e.g. 1.7% Basalt from El Hierro volcano) the decrease in P-wave velocity is particularly high, varying from a 96% of initial (unfractured) velocity to 87% for raypaths at an oblique angle of 4 degrees to the failure plane. Conversely, velocity decreases for the other rocks (of higher initial porosities), whilst decreasing by 7%–8%, did not exhibit such a large decrease regardless of raypath angle (Fig. 4). In all cases, the velocity anisotropy (difference between lowest and highest wave velocities) increases markedly by the end of the experiment, due to the preferential alignment of the damage zone. The use of such data is useful as it acts as a control or calibration for methods that employ seismic tomography and reflection seismic data to understand the subsurface volcanic plumbing system (e.g. Refs. 86, 92, 93).

(ii) Induced seismicity due to shear fracture, fluid-rock interaction, and fluid-turbulence

With a fracture established, regardless of setting or system, it is natural to consider the fluids present, as the majority of crustal rocks are fluid saturated.[94] When fluids move rapidly through fractures and cracks, as widely postulated in active geological areas, swarms of seismic events are often recorded. Early evidence for so-called "tremor" was first noticed in and around active volcanoes where the method was once thought to herald a new and more accurate method to forecast volcanic unrest.[12,33,95] Later studies have now found similar fluid-triggered seismicity in other tectonically active areas, such as in subduction zones where they are often referred to as "non-volcanic" tremor.[8,16,75,85,96,97] Using the laboratory methods of Benson et al.[15] and Fazio et al.[34] there is clear evidence that these swarms are generated by a complex combination of the fluid-mechanical response of the system, and the effects of fluids decompressing and resonating through fractures and conduits in the rock mass.[98] Fig. 5 shows typical data from such an experiment, where high fluid flow is induced by rapidly venting a high pressure pore fluid (water) via an electrically operated solenoid valve (Fig. 5A–C; Benson et al.[15]; Fazio et al.[34]). During the venting stage, a clear swarm of acoustic emission is seen, and linked to the damage zone.[15] Furthermore, recent data suggests a link between the phase (or viscosity) of the fluid and the resonance frequency recorded during the swarm stage of the experiment.[34] The complex rock-fluid coupled system also generates very specific signals known as tornillo events[98–100] that are characterized by long coda of decreasing amplitude (Fig. 5D). These signals were amongst the earliest evidence for rock-fluid driven seismicity measured by volcano seismologists, and have now also been simulated in the laboratory,[69] shown in Fig. 5(D–E).

Here, during fluid decompression at 175 °C (from a pore pressure of 10–16 MPa to 0.1 MPa) via an electrically operated valve, a swarm of AE events was recorded, continuing for several 10's of seconds in a number of discrete swarms after this initial pressure decrease (or 'venting') stage. This is longer than a typical decompression experiment at 'room' temperature as shown in Fig. 5C.[34] This type of effect has clear application in the area of geothermal energy, as the process of resource extraction (implying decompression) will – by definition – require fluids to be received at a well, after moving through a damage zone at high flow rates, changing the state of stress of the crust and thus likely to stimulate a local seismic response. The use of field data is established in many geothermal areas for such monitoring of production. Induced seismicity also includes scenarios whereby pore fluids are sufficiently high to locally fracture rocks in tension. In volcanic areas, this is seen in the form of veining and dyking and is a natural extension and compliment to the fluid-flow experiments above.

(iii) Induced seismicity due to tensile fracture, fluid flow, and permeability

The counterpoint to the seismic response of shear faults and rapid fluid flow (turbulence) is the effect of fluid overpressure to generate stress sufficiently high to fracture rock directly. In

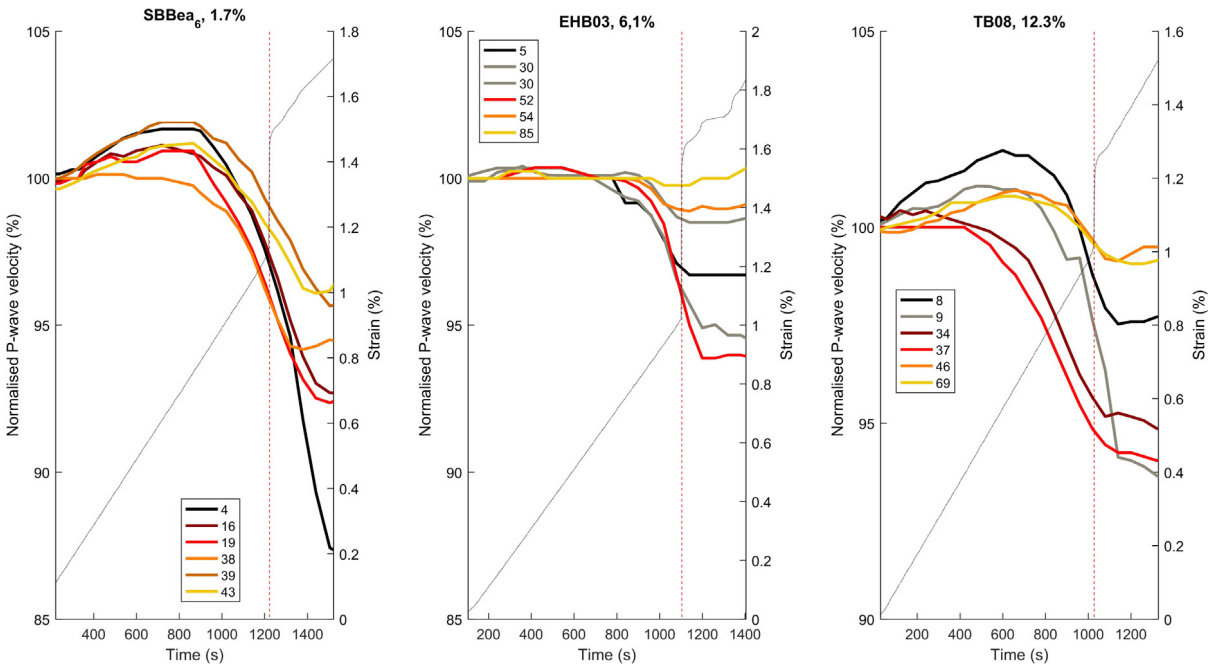

Fig. 4. Normalized P-wave velocity as a function of damage formation during standard triaxial deformation experiments for a basalt from Stromboli, El Hierro and Tenerife volcanic island (after Ref. 89). In all cases the velocity decreases significantly as the shear plane is formed, with raypath angles at a shallow angle to the shear plane undergoing more significant normalized decreases compared to raypaths at high incidence angles.

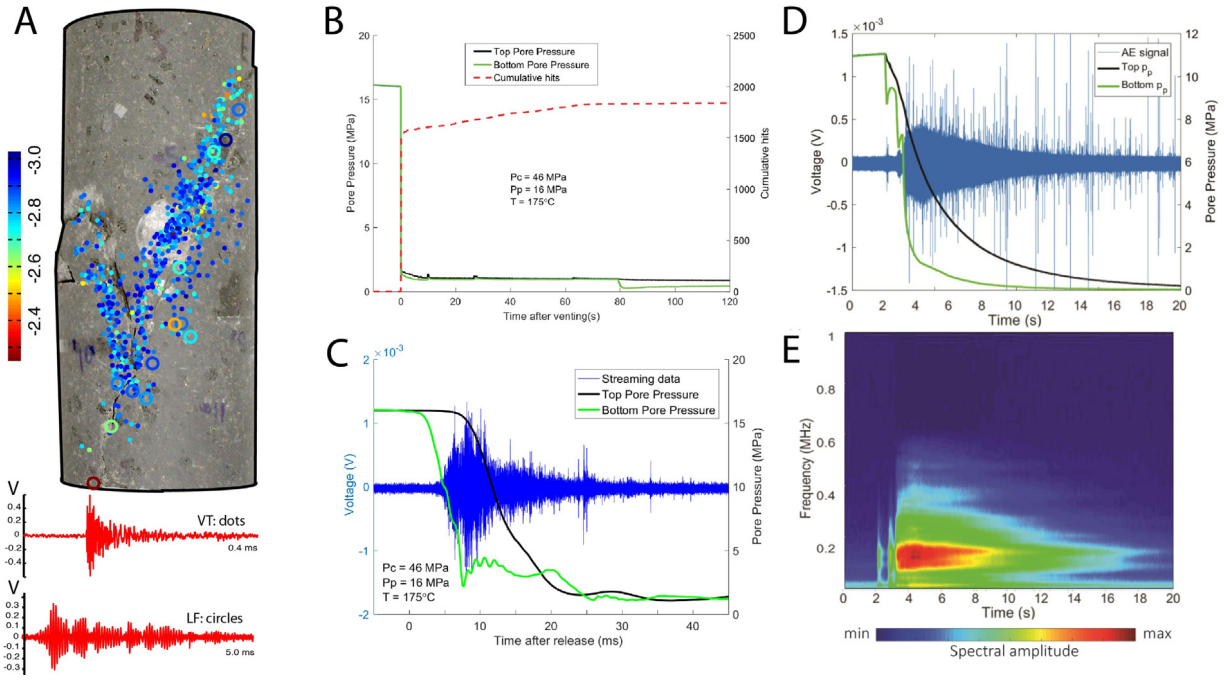

Fig. 5. Induced laboratory AE events in fractured Etna basalt from, (A): fracture (VT) events and direct fluid (LP events) movement in a shear (damage) zone; (B): fluid venting induced AE and (C) AE from fluid movement of a multi-phase mixture (water and steam) due to fluid depressurization at elevated temperatures. Finally, (D) Long coda waveform and (E) monochromatic spectrogram characteristic of tornillio events. After Refs. 15, 34, 69.

volcanic areas, this commonly results in extensive dyking.[63] Although these processes have been simulated in the laboratory, the extremely high temperatures required to simulate volcanic related processes pose unique challenges as equipment cannot easily control or measure geophysical data of such processes, despite a small number of attempts (e.g. Refs. 59, 101). To overcome the issue of temperature, analogue experiments using a setup similar to that described in Fig. 2C have successfully reproduced the effects of hydraulic fracture but using softened PMMA. At elevated temperature (175 °C) and pressure (30 MPa) a PMMA rod, simulating an intruding magma body, behaves as a viscous liquid under these conditions (Fig. 6).[62] Data from these experiments shows that the pressurized conduit exerts a radial stress on the inner bore of the outset country rock until fracture (Fig. 7). The accompanying AE trend initially increases very slowly up to approximately 800 s, after which the AE trend increases exponentially until a decrease in conduit overpressure (rock failure) is recorded at 1000 s, the same time as the peak in AE hit rate.

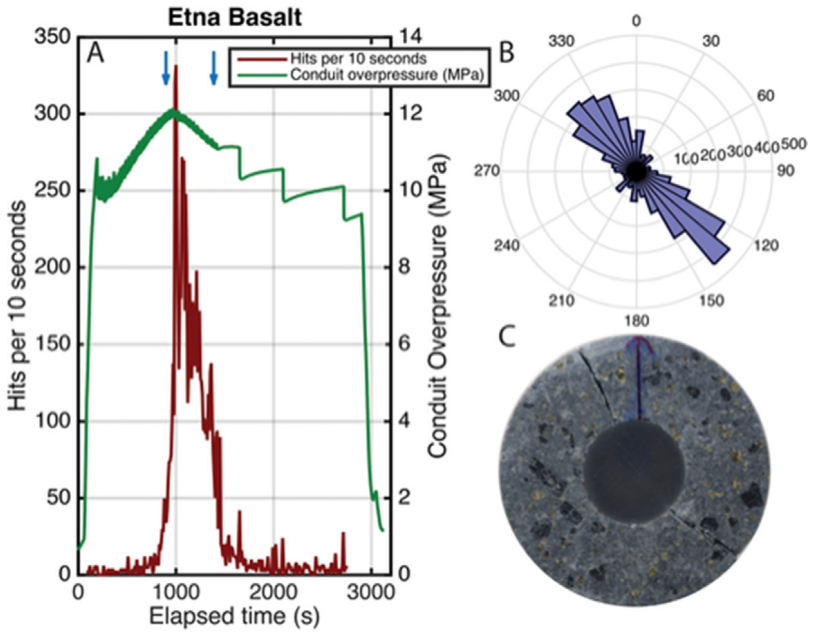

Fig. 6. Panel A: Conduit overpressure and AE hit count during pressurization of a heated conduit filled with PMMA. Panel B: 2D locations agree well with the post-test fracture position (Panel C). After Ref. 62.

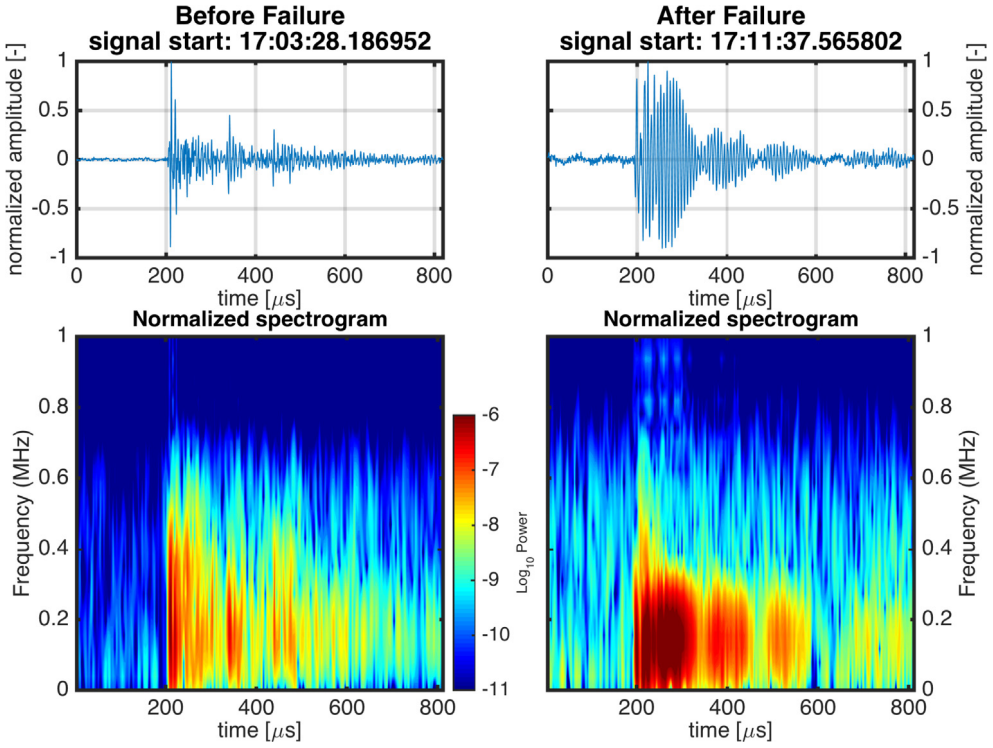

Fig. 7. Comparison of Acoustic Emission waveforms recorded during (left panel) and after (right panel) the injection of molten PMMA from a central conduit into the surrounding think-walled cylinder of rock. This is analogous to tensile fracture and then fluid movement through the newly generated tensile cracks. After Ref. 62.

Although the presence of the large axial conduit precludes 3D location, a radial fracture density map may still be generated (Fig. 6B) which matches well to the fractures observed post-test. Finally, it is noted that fractures not only are filled with the post-test hardened PMMA but, as the PMMA intrudes post fracture, a lower frequency waveform trend is recorded (Fig. 7B[62]). This is consistent with the earlier data from water/steam decompression.

This method is similar to the 'thick walled cylinder test' and has been used to simulate fluid-driven tensile fracture (e.g. Ref. 71), also known as hydraulic fracture. Fig. 2C shows the general principle as reported by Gehne et al.[53] which uses two steel water guides fitted with a series of O-rings to seal a central conduit which is pressurized with water. When water is pumped at a constant flow rate (1 ml/min) into the central cavity, pore fluid pressure builds up, eventually overcoming the natural tendency of the sample porosity and permeability to remove the pressure build-up, until sample failure. Due to the competition between fluid flow and the country rock permeability, the

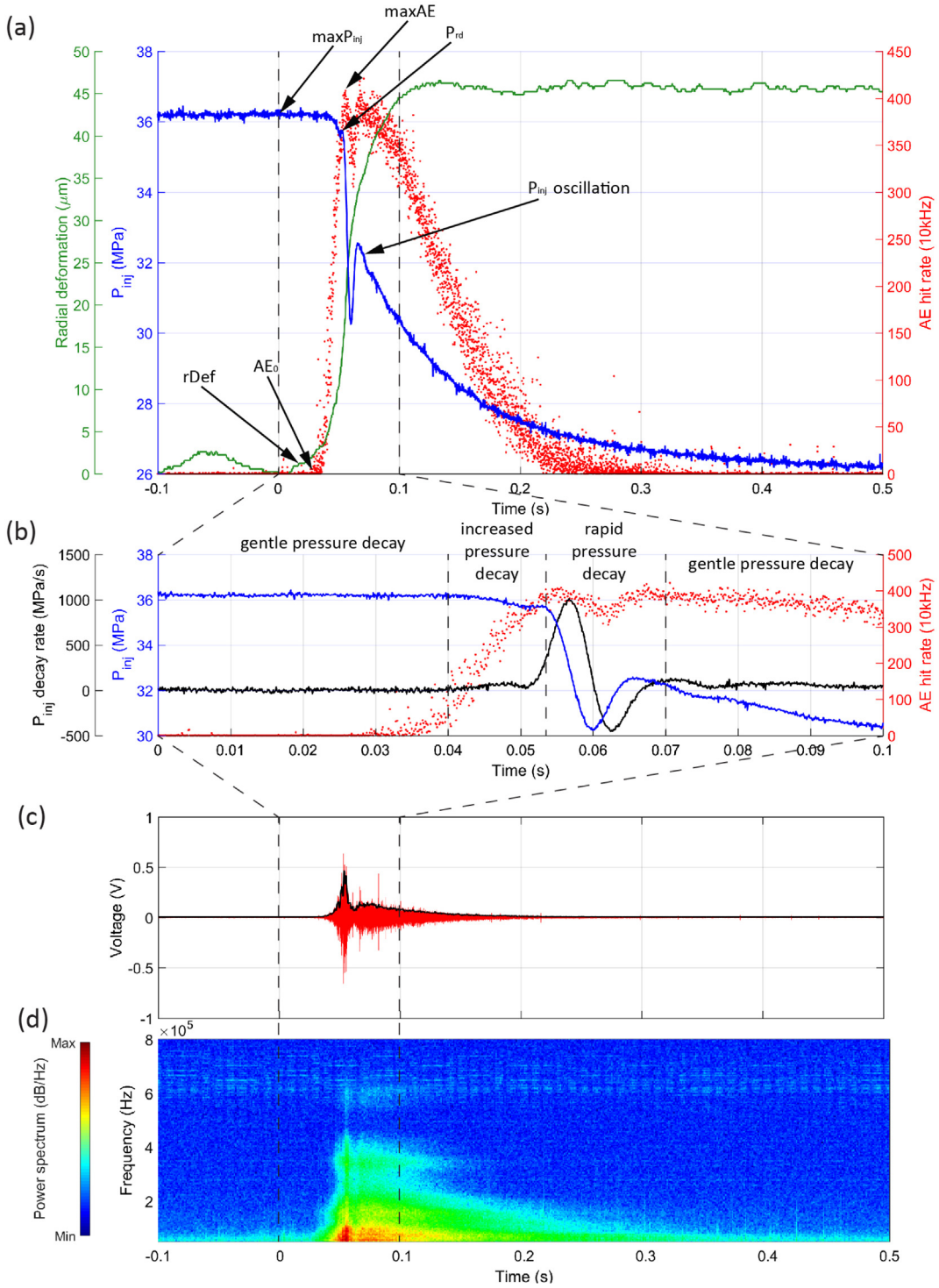

Fig. 8. Laboratory data obtained at a confining pressure of 25.4 MPa in the anisotropic Nash Point Shale cored with bedding parallel to sample axis; (a) Time-record of internal fluid injection pressure (blue line), radial deformation (green line) and AE hit counts (red dots). (b) Fluid pressure decay rate (black line), fluid pressure (blue line) and AE hit count rate (red dots). (c) Snapshot of the continuous waveform (red line) including the signal envelope at the time of failure. (d) Respective spectrogram at the time of failure. The spectrogram data illustrates the frequency range exhibiting power (colour) with time. Time scales zeroed at maximum fluid injection pressure. After Ref. 53.

method works well for low permeability samples with permeabilities lower than approximately 10^{-15} m^2. Data is collected using radial and axial strain gauges, a network of 11 AE sensors, and mechanical and pore pressure transducers, all sampling data at a rate of 10 kHz. An additional pore fluid pressure sensor is sampled at the highest data acquisition rate of 10 MHz by using a channel of the continuous AE recorder with suitable signal conditioning. This allows a very high temporal resolution experiment to be synchronized in time. A typical dataset is shown in Fig. 8.

Simulating hydraulic fracturing using water as pore fluid and silicone oil as confining pressure, at 25.4 MPa representative of a burial depth of approximately 900 m, results in tensile fracture at a breakdown pressure just over 36 MPa. Defining the time of maximum pore fluid pressure, P_{inj}(max) of 0 s, radial strain

first increases slowly up to 0.04 s and then accelerates rapidly to 25 μm at approximately 0.06 s after breakdown pressure. This is preceded slightly by a supra-exponential increase in AE activity which reaches a maximum at around the same time (0.05 s). Fluid pressure decay rate increases significantly at 0.035 s from an average of less than 20 MPa/s to a maximum of over 1000 MPa/s at 0.055 s. Also noticeable is a pore fluid oscillation or "bounce" with the pore fluid pressure recovering from a minimum of approximately 30 MPa to approximately 32 MPa, before decreasing again, likely due to the fluid being unable to keep up with the freshly generated advancing fracture.[53] This behaviour appears to be limited to lower confining pressures (approximately 6 MPa and lower) and is not seen at higher pressure (above approximately 12 MPa), as reported by Gehne (2018).

The AE activity mirrors the fluid pressure (an oscillating pattern), but with a very small time offset (≈0.005 s). The continuous signal (Fig. 8C) illustrates the nature of the signal as a series of short bursts during the fracturing event, which initially has a very brief high frequency component at the initial fracture event but which then quickly give way to a low frequency and impulsive onset, and a short and fast decreasing tail. The most significant power is in the range 50–200 kHz (Fig. 8D), but a higher frequency component occurs at 400 kHz. The lower frequency component is fairly continuous, and we note that the high frequency components appear as shorter bursts or swarms. Following the oscillation, fluid pressure dissipates gradually from 0.15 s and the radial strain increases significantly, signalling the end of the experiment at around 0.2 s.

Although these data show the effect of increased confining pressure (burial depth) on the tensile strength (and strength anisotropy) of the rock, it does not consider the connected porosity and therefore permeability. However, by making an additional modification to the setup in Fig. 2D, it is possible to estimate the flow and therefore permeability of the freshly generated fracture, as reported by Gehne and Benson.[74] For Nash Point Shale, a low porosity shale of initial permeability in the range 10^{-18} to 10^{-20} m^2, the fracture event increased the apparent permeability to between 2×10^{-15} to 2.5×10^{-16} for effective pressures from 2.5 to 25 MPa respectively, and which does not recover when the effective pressure is decreased. Such permeability hysteresis was shown to be particularly evident in the Crab Orchard Sandstone (due to the presence of cracks and clays) as reported by Gehne and Benson,[48] and shown in Fig. 9. This tight sandstone,[102] has a porosity of approximately 5%, a nominal permeability in the micro-Darcy (10^{-18} m^2) range and a significant anisotropy generated by mm scale cross-bedding: up to 20% using P-wave elastic velocities, and nearly 200% in terms of permeability anisotropy.

As shown in Fig. 9, for Crab Orchard sandstone parallel to bedding an initial permeability of 33×10^{-18} m^2 is measured, and for flow normal to bedding, 2×10^{-18} m^2 both at an effective pressure of 5 MPa. As effective pressure is increased an exponential decrease in permeability is recorded for flow in both orientations, however for flow parallel, this reaches a 'floor' of around 10×10^{-18} m^2. For flow parallel to bedding, the permeability does not increase (recover) with subsequent reduction in effective pressure, and this general pattern is seen in the second full cycle, decreasing to a minimum of 1×10^{-18} m^2. For a third (partial) cycle this minimum was maintained in both increasing and decreasing effective pressures. For flow normal to bedding, even though the permeability k is lower overall, the flow does recover slightly, such that the permeability anisotropy $(k_{max} - k_{min})/k_{mean}$ actually decreases significantly during the second half (decreasing pressure) of the second cycle, and then is maintained in successive cycles at approximately 25%, due to the permeability of normal fluid flow of approximately 1.5×10^{-18} m^2. Both are evident from the AE and fluid injection pressure which suggest

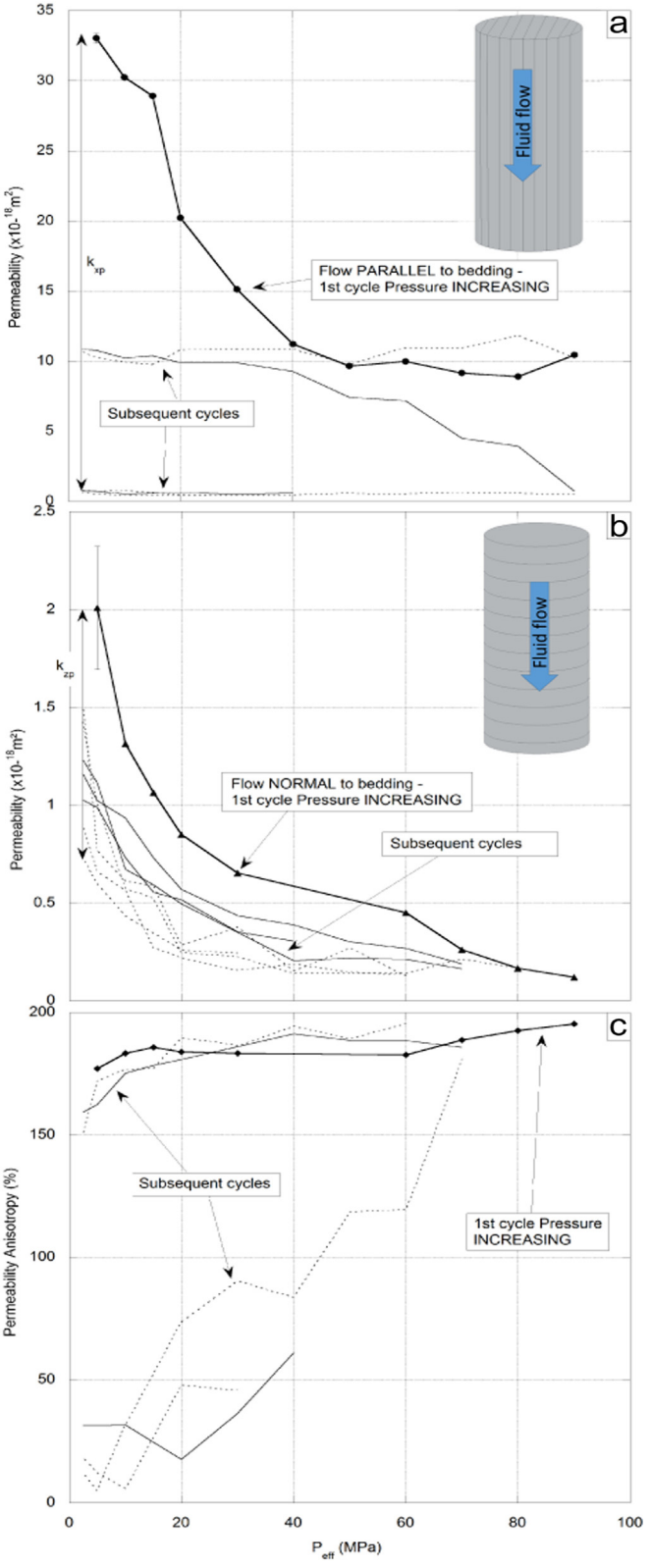

Fig. 9. Permeability parallel to bedding (panel A), normal to bedding (panel B) and permeability anisotropy (panel C) evolution in Crab Orchard sandstone over an effective hydrostatic pressure range up to 90 MPa; k_{xp} and k_{zp} indicating the permanent permeability change — (a) k_x, (b) k_z, (c) A_k. Effective pressure increase is shown with solid lines, decrease with dotted lines, and with the initial increase as a thick black line.
Source: From Ref. 48.

Table 1
Simplified rock physics data of the rock types reviewed in this study. Note permeability data is not available for TB and EHB as this was not an important aim of the Harnett[89] study. In the case of NPS and COS, the anisotropy due to the bedding/fabric produces noticeable permeability anisotropy with typical low (normal to bedding) and high (parallel to bedding) values cited.
Source: Taken from Refs. 34, 48, 53, 89.

Property	Etna Basalt (EB)	Stromboli Basalt (SB)	Tenerife Basalt (TB)	El Heirro Basalt (EHB)	Dumaguete Andesite (DA)	Nash Point Shale (NPS)	Crab Orchard Sandstone (COS)
Porosity, %	2.1	6.1	12.3	1.7	6.0	6.3	7.1
Initial Permeability (m^2)	10^{-16}	6×10^{-16}	n/a	n/a	1.5×10^{-16}	10^{-18}–10^{-21}	$2–33 \times 10^{-18}$
P-wave anisotropy, %	1.0	2.0	1.8	2.2	1.0	56.0	20.0

that variations on pore fluid may significantly (and permanently) change the bulk permeability, and therefore resource potential, of fractured reservoirs such as those often used in engineered geothermal and unconventional hydrocarbon industries.

These are important details, as no unconventional hydrocarbon or geothermal reservoir will be effective if pore fluids (water, hydrocarbons) cannot flow easily enough through the rock mass to a receiving well. And, whilst flow might be high initially, there are well documented cases of flow rate significantly decreasing over time, for both geothermal production and for unconventional hydrocarbon extraction. Many causes are inferred, such as mineralogical alteration within the pore space and cycling of the pore (production) pressure with time, which have the effect of changing the flow through the rock mass via mechanical changes. Such effects often require an unconventional reservoir to be re-fractured at key future stages in the lifetime of the resource (e.g. Ref. 103). Laboratory data suggest that the permeability of a tight rock formation may decrease significantly if the effective pressure (difference between confining pressure and pore fluid pressure) is allowed to increase and decrease through time.[48] Whilst the range of pressure change investigated here were higher than a typical field scenario (ranging from 5–90 MPa), the reduction in permeability was found to be not recoverable in subsequent cycles, and that the main reduction occurred in the first 20 MPa of pressure change. The inherent anisotropy was a significant factor in determining the permeability and permeability hysteresis.[48,74]

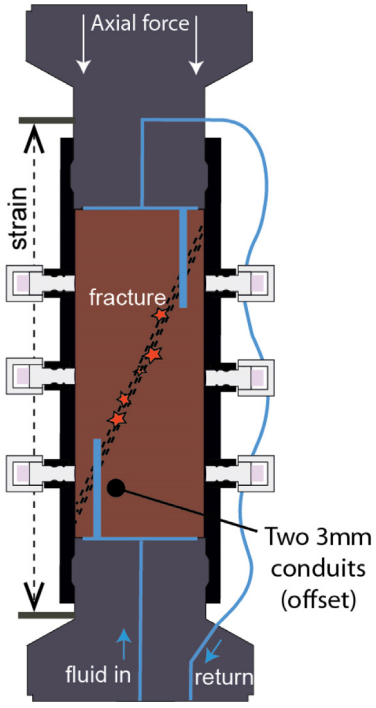

Fig. 10. Modified setup for flow measurement along a naturally generated fault plane generated using a triaxial cell, using two offset drill-holes to inject and receive fluids along the fracture plane generated due to axial deformation under triaxial conditions.

4. New data: fracture, flow, and induced seismicity from a study using Dumaguete andesite from the South Negros geothermal field, Philippines

To compliment the review of data and methods above, we here also report a short study using a variation of the setup shown in Fig. 2, simulating fracture and fluid flow along an inclined, newly generated, shear fracture. The rock used is a Dumaguete Andesite (DA) from the Philippines (supplied by Energy Development Corporation) from a borehole in the Southern Negros geothermal field. Key properties for the material are tabulated below alongside the other rocks reviewed for completeness. As shown in Fig. 10, a set of two offset 3 mm drill holes intersect the top and bottom of a newly generated fault (due to triaxial deformation), the orientation of which is further promoted to intersect these drill-holes via 'notches' on the outside of the sample and filled with sand/cement to avoid piercing the jacket. This allows measurement of fracture permeability and P-wave velocity to be made as a function of confining pressure, simulating burial depth , and up to 175 °C (see Table 1).

Fig. 11 shows P-wave velocity data, dynamic Poisson's ratio, and Dynamic Young's modulus (i.e. derived from velocity data) from the Dumaguete andesite during triaxial deformation, forming the initial shear fault. We note a similar velocity trend to that seen in Fig. 4, with an increasing velocity as the specimen is deformed, from 5500 m/s to 5800 m/s, followed by a sharp decrease at the point of failure (generation of a shear fault). Post failure, the velocity steadily increases with strain (time). The dynamic Poisson's ratio shows a steady increase with strain until sample failure, at which point a significant increase is recorded, after which Poisson's ratio decreases steadily. Finally, the dynamic Young's modulus shows a trend similar to that of P-wave elastic velocity with a sharp decrease at point of failure, followed by a recovery phase. Taken together, it is likely that such data, if remotely collected and monitored in the field, has the potential to provide operators with useful information as to whether a geothermal reservoirs have new fractures opening, or whether pressure/stress levels are acting to close the fracture and associated damage zone. These results are consistent with stress cycling experiments showing similar trends in elastic moduli as damage is incrementally induced.[104] To evaluate the static Young's modulus, a number of small stress cycle loops were made after the development of the shear plane at increments of 5 MPa confining pressure. Fig. 12 shows these data, also evident in the time record in Fig. 11 from 4000 s onwards. We measure little change in static Young's modulus with increasing confining pressure for positive stress loops (increasing strain), whereas a steady increase in modulus is calculated when taking the negative (decreasing strain) portion of the stress–strain loop.

To exploit conventional geothermal resources, some form of permeable conduit is needed. In the field, this may be achieved by drilling producer wells into an area where deep geothermal

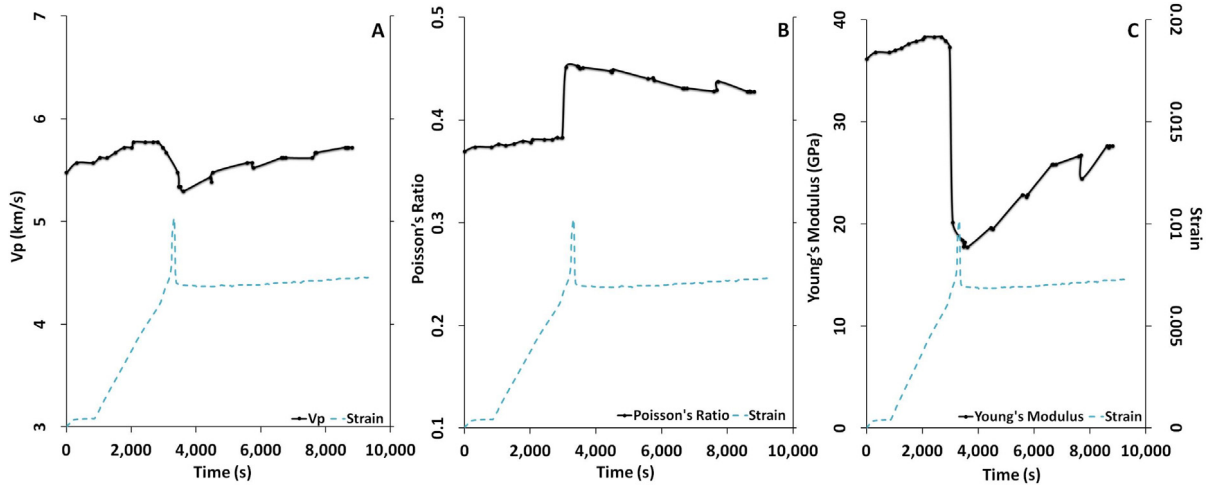

Fig. 11. P-wave velocity (Panel A), dynamic Poisson's ratio (Panel B), and dynamic Young's modulus (Panel C) of the Dumaguete andesite from the Southern Negros Geothermal field (near Dumaguete city) during conventional triaxial deformation deformed at 6.1 MPa confining pressure. The blue dashed line shows the concomitant change in strain during the experiment (constant strain rate triaxial test).

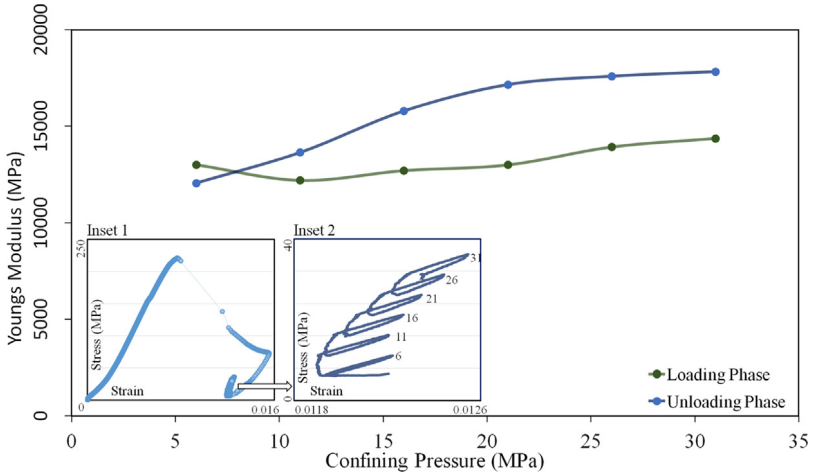

Fig. 12. Change in static Young's modulus of Dumaguete andesite. Each data point was derived after the shear plane has been generated after the sample failure (inset 1), by increasing stress due to a strain rate until a maximum of 10%–20% of the failure shear stress (220 MPa) is achieved, before unloading. This was repeated 6 times (inset 2). The Young's modulus was derived by applying a best-fit line to the stress–strain data. This procedure was then repeated for decreasing portions of the stress loops (inset 2).

fluids are already present, or via the development of engineered geothermal systems. In the former case, examples include the extensive Hellishedi geothermal field (Iceland), and the Southern Negros geothermal field in the Philippines. Using the dual-offset conduit method (Fig. 10) and applying a differential pressure across the two drill holes, we performed a series of fluid flow experiments to determine permeability, shown in Fig. 13. The flow rate through the shear zone decreases from 7.7 μl/s at 5 MPa, to less than 0.03 μl/s at 30 MPa, and shows a sharp decrease in flow rate as pressure is increased from 5 to 15 MPa.

By ascribing this to a notional "slot" that connects the two conduits, it is possible to measure a permeability via Darcy's law (Fig. 13) using $k = (Q/A)(\mu L/\Delta P)$, where k is permeability, Q is the measured volume flow rate, A is the slot area (thickness x fixed width of 40 mm), μ and L the fluid viscosity and fracture length, and ΔP the pressure differential. For a slot thickness of 0.2 mm, the equivalent permeability decreases from approximately 1.35×10^{-14} m^2 at 5 MPa effective pressure to only 0.25×10^{-15} m^2 at the maximum effective pressure of 30 MPa. Higher values of slot thickness (0.4 mm, 0.6 mm) produce a concomitant decrease in permeability, with a value of 0.2 mm fitting well to the data. The permeability of unfractured DA is extremely low, less than 1.5×10^{-16} m^2, which is similar to Etna Basalt. We attribute this to the poorly connected porosity of these volcanic rocks. As noted earlier, an ongoing challenge related to both geothermal and also unconventional resource extraction is that of permeability hysteresis. Cyclical pore (or effective) pressure is known to have serious effects on the ability of a fracture network to recover to a previous value of permeability (hysteresis effect), as measured on low porosity sandstone (5%). We attribute this effect in DA to the presence of clay and other minerals in the crack fabric of this rock type (long, thin, high aspect ratio cracks) that are less resilient to pressure than equant pore space.

In addition, hysteresis is found to impact elastic wave velocities and moduli. The highest fracture permeability (after sample deformation) was at low confining pressures. This coincides with a significant reduction in P-wave elastic velocity and Young's modulus. Conversely, the subsequent increase in confining pressure resulted in a partial recovery of elastic attributes but with considerable reduction in permeability. Static moduli acquired via mechanical stress–strain loops follows a similar trend. The behaviour of the examined properties is likely to reflect the

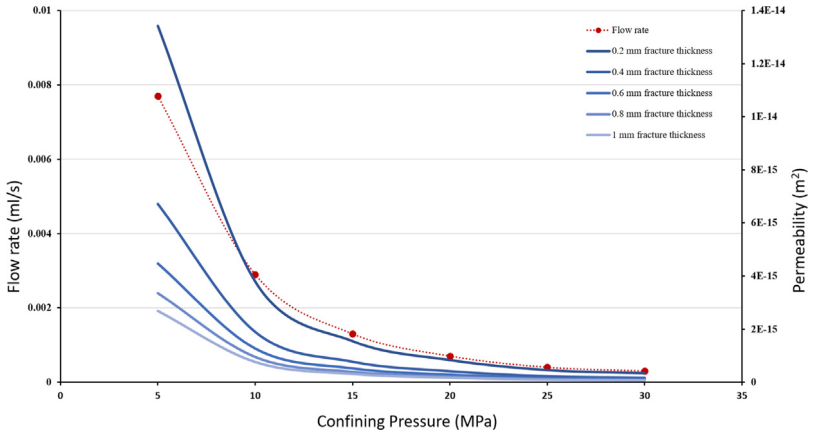

Fig. 13. Permeability data for a freshly generated (simulated *in-situ*) shear fracture linking two offset conduits, simulating fluid-stimulated geothermal systems. The calculated permeability, based on measured flow rate and modelled by a parallel slot lining the injection and receiving ports, is primarily controlled by the cumulative crack aperture. Permeability decreases both with increasing confining pressure, and with subsequent cycles of confining pressure.

changing material competency (elastic properties), and is potentially useful in interpreting seismic models of geothermal systems where changes in physical conditions can occur rapidly which have severe implications to the economic sustainability of the reservoir. New fractures, and movement on existing faults, are manifested as both large and small magnitude earthquake swarms commonly occurring in tectonically active areas where geothermal fields are situated. Therefore, movement and the onset of rock mass instability could be detected by monitoring the behaviour of seismic attributes modelled from surface seismic instruments, with the aim of avoiding reactivation of dormant structures such as in the Basel event (Switzerland: Giardini[30]; Bachmann et al.[31]) and the Presse Hall triggered sequence (UK: O'Toole et al.[105]; Clark et al.[24]). The ability to detect and monitor fracture permeability hysteresis will be particularly helpful in resource management by determining which part of the reservoir can be further exploited and targeted for drilling production wells.

Finally, the sample was heated to 175 °C and the pore fluid (water) vented to stimulate AE. Fig. 14 shows the AE signal, which is generated, due to the modified setup, by fluid travelling along the damage zone and associated shear fault. The AE shows the same low-frequency response at the onset of fluid decompression as reported by other studies[15,34] due to the rock-fluid coupling. We also note that AE data shows a longer lasting waveform, compared to the previously used Etna basalt which we attribute to the higher porosity of this material (6%, compared to 2% for Etna basalt). This, combined with the development of a more extensive damage zone linked by the offset conduits, likely generates conditions whereby fluid is able to vent more slowly through the fracture damage zone to atmosphere and thus yielding the longer tremor in the AE record. Such data have been instrumental in covering the key gaps in knowledge between these natural systems and the engineered environment. And, although the difference in scale is obvious, scale invariant methods such as AE location and elastic wave velocity changes map well to fault shear zones, across a range of controlled conditions (e.g. Ref. 15). The seismo-mechanical relationship during hydraulic fracturing shows that AE activity can generate a useful geophysical picture of the evolving tensile fracture nucleation in crustal rocks allowing laboratory experiments to generate data that help to develop our understanding of fracture in the field, and how seismicity can be used to better understand and monitor the process remotely. Such warning methods are also widely used in the mining industry where it is used to guide the process, often for safety reasons (e.g. Collins et al. 2002).

5. Discussion and conclusions: coupled hydro-mechanics in energy geosciences

Many areas of geomechanics for energy and resource exploration rely on fluid flow in porous media for their viability, ranging from conventional hydrocarbon and water reservoirs, to unconventional hydrocarbons and engineered geothermal systems. In the case of unconventional hydrocarbons and geothermal systems it is often necessary to generate new shear and tensile fracture networks in order to fully exploit these resources, in addition to the reactivation of pre-existing discontinuities. A number of natural fracture systems have been reported where there is evidence for fluid-driven fracture (e.g. Ref. 63). This is evident in the field of volcanology, for example, where dyke and magma intrusions are a good analogue for natural hydraulic fracture — even though the pressure and temperatures are very high. The processes of dyke intrusion and hydrothermal fluid injection are known to produce a diverse range of seismic activity depending on the model of rock fracture, or the nature of the fluid resonance within the fractured media (e.g. Chouet et al., 1996). The monitoring of local seismicity in and around volcanoes has been used for decades to better understand the deep volcanic processes and plumbing system. The increasing event rate and magnitude of volcano-tectonic activity has often been used to forecast impending unrest and is now a standard tool in most volcano observatories (e.g. Refs. 32, 106–108). In the early 1980's this was joined by the discovery of Low Frequency and Long Period signals due to fluid resonance and turbulence that, for a time, was thought to herald a new era of forecasting (e.g. Ref. 33). However, this has not transpired due to the complexities of these natural systems.

Understanding the physical properties governing fluid-rock interactions and permeability is critical to the development of energy resources previously not sought after due to complexities and lack of knowledge. Here, using laboratory methods and rock samples taken from the field in areas spanning both geothermal and hydraulic fracture potential allows us to collect seismic, mechanical, and fluid flow data contemporaneously. Properly conducted, such calibrations will elucidate the underlying processes by simulating subsurface conditions. We have here reported both legacy hydraulic fracture data, and new data focusing on the geothermal potential of the Southern Negros geothermal field. From these, we conclude that the delay in unstable fracturing is related to fracture geometry and the complexity of the fracture network, as revealed by longer delay phases in experiments with more complex fracture geometries. In the case of fluid-driven

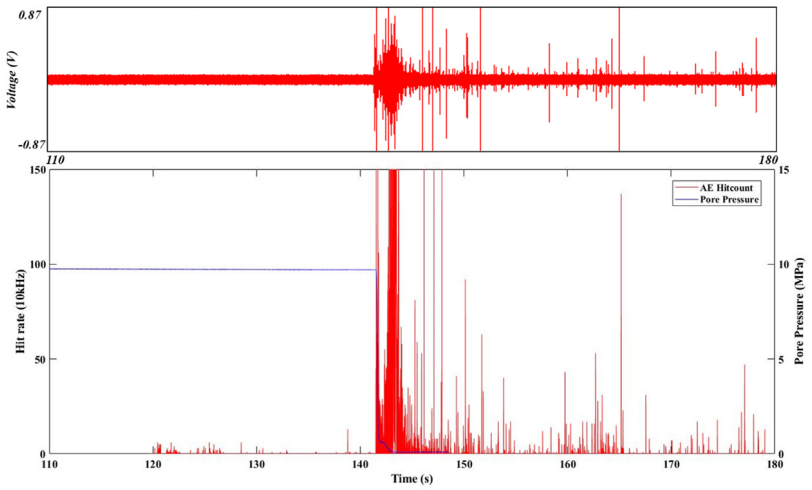

Fig. 14. New data showing AE swarms recorded in Dumaguete Andesite as pore fluid heated to 175 °C is vented through the damage zone geometry as shown in Fig. 1(C). In a similar matter to Fazio et al.[34] a swarm of AE is recorded as pressure is vented, which continues as liquid water changes to steam.

tensile failure, once sufficient pressure has built up fracture propagation evolves from a stable to an unstable regime, marking the breakdown of the sample. Combined, these new laboratory simulations provide an alternative view to the widely applied assumption that both events occur at maximum fluid pressure. These observations show that AE activity, fluid injection rates, and deformation are key indicators for estimating rock fracture subjected to elevated fluid pressures.

Fluid production in geothermal fields causes a decrease in pore pressure that in turn promotes the occurrence of cold-water intrusion and steam cap development. Specifically, the relatively rapid decrease of pressure around production wells creates a depression in the pressure profile and enhances two-phase (liquid and steam) fluid formation. We find that this liquid–gas phase change generates characteristic and persistent AEs at low frequencies (10–90 kHz in the laboratory). This transition occurs at a pressure (around 2 MPa) at which water no longer remains in the liquid phase at the temperature tested of 175 °C,[109] and consistent with typical geothermal reservoir conditions. Studies simulating fluid movement in volcanic areas have reported similar findings, revealing that events generated from pressure release at high temperatures differ from shear fracturing induced events when analysed in terms of source (focal) mechanisms (e.g. Julian 2012; Gomez et al., 2014). Such analyses have also been used to evaluate mining stability (e.g. Collins et al. 2002). Specifically, pure-fluid-turbulence seismic swarms are found to be dominated by compensated linear vector dipole (CLVD) type of events while fracture and fault-slip consist mainly of double couple (DC) events (e.g. Ref. 41). This highlights the usefulness of acquiring seismic data in producing geothermal/unconventional fields to identify areas undergoing processes described above that are critical to managing geothermal resources. Discriminating such fluid-induced seismicity from fault generated natural seismicity has the potential for geohazard applications as well as finding new areas to develop wherein active faults can be identified. The combined extraction and injection of fluids in geothermal energy development alters the natural seismicity of the area. It is widely known that fluid-injection creates earthquakes by increasing pore pressure and driving already critically-stressed faults and fractures to failure. Using recent data using samples taken from an existing geothermal reservoir, it would appear that fluid extraction also contributes to seismicity by means of pore pressure decrease, causing fluid movement and fluid phase change.

Finally, we note that fracture permeability has been studied using different geophysical methods with the aim of better guiding exploration and development of energy resources. These geophysical methods make use of a number of physical properties (e.g. resistivity) that provide information on the state of the rock mass. By highlighting how seismic attributes change with external stimuli (pressure, temperature), clues to the evolving permeability of the deep rock mass might be estimated from field-based geophysics methods.

Declaration of competing interest

The authors declare that they have no known competing financial interests or personal relationships that could have appeared to influence the work reported in this paper.

CRediT authorship contribution statement

Philip M. Benson: Conceptualization, Methodology, Funding acquisition, Project administration, Writing - original draft, Writing - review & editing. **David Carlo Austria:** Formal analysis, Writing - original draft. **Stephan Gehne:** Methodology, Formal analysis. **Emily Butcher:** Methodology. **Claire E. Harnett:** Methodology, Writing - original draft. **Marco Fazio:** Methodology, Formal analysis. **Pete Rowley:** Formal analysis, Project administration, Writing - original draft, Writing - review & editing. **Ricardo Tomas:** Formal analysis.

Acknowledgements

This work has been financed by the National Environmental Research Council (Grant No. NE/L009110/1), a Marie Skłodowska-Curie Reintegration grant (contract No. 333588), and a Royal Society equipment grant (Grant No. RG130682) to PMB. The CT scanning has been performed in the Future Technology Centre at the University of Portsmouth.

References

1. Scholz CH. Fault mechanics. In: *Treatise on Geophysics, Vol. 6*. Elsevier; 2007, p. 441–483. http://dx.doi.org/10.1016/B978-044452748-6.00111-5.
2. Faulkner DR, Mitchell TM, Healy D, Heap MJ. Slip on 'weak' faults by the rotation of regional stress in the fracture damage zone. *Nature*. 2006;444:922–925. http://dx.doi.org/10.1038/nature05353.
3. Guéguen Y, Palciauskas V. *Introduction to the Physics of Rocks*. Princeton University press: New Jersey; 1994, p. 292.

4. Paterson M, Wong T-F. *Experimental Rock Deformation: The Brittle Field*. Springer: Berlin; 2005, http://dx.doi.org/10.1007/b137431.
5. Etheridge MA, Wall VJ, Cox SF, Vernon RH. High fluid pressures during regional metamorphism and deformation: Implications for mass transport and deformation mechanisms. *J Geophys Res: Solid Earth*. 1984;89(B6):4344–4358. http://dx.doi.org/10.1029/jb089ib06p04344.
6. Tarling MS, Smith SAF, Scott JM. Fluid overpressure from chemical reactions in serpentinite within the source region of deep episodic tremor. *Nat Geosci*. 2019. http://dx.doi.org/10.1038/s41561-019-0470-z.
7. Llana-Funez S, Wheeler J, Faulkner DR. Metamorphic reaction rate controlled by fluid pressure not confining pressure: implications of dehydration experiments with gypsum. *Contrib Mineral Pet*. 2012;164:69–79. http://dx.doi.org/10.1007/s00410-012-0726-8.
8. Dragert H, Wang K, James TS. A silent slip event on the deeper Cascadia subduction interface. *Science*. 2001;292:1525–1528. http://dx.doi.org/10.1126/science.1060152.
9. Milsch HH, Scholz CH. Dehydration-induced weakening and fault slip in gypsum: Implications for the faulting process at intermediate depth in subduction zones. *J Geophys Res*. 2005;110:B04202. http://dx.doi.org/10.1029/2004JB003324.
10. Tuffen H, Dingwell DB. Fault textures in volcanic conduits: evidence for seismic trigger mechanisms during silicic eruptions. *Bull Volcanol*. 2005;67:370–387. http://dx.doi.org/10.1007/s00445-004-0383-5.
11. Tuffen H, Smith R, Sammonds PR. Evidence for seismogenic fracture of silicic magma. *Nature*. 2008;453:511–514. http://dx.doi.org/10.1038/nature06989.
12. Chouet BA. Ground motion in the near field of a fluid-driven crack and its interpretation in the study of shallow volcanic tremor. *J Geophys Res*. 1981;86:5985–6016. http://dx.doi.org/10.1029/JB086iB07p05985.
13. Chouet B. Long-period volcano seismicity: Its source and use in eruption forecasting. *Nature*. 1996;380:309–316. http://dx.doi.org/10.1038/380309a0.
14. Burlini L, Vinciguerra S, Di Toro G, De Natale G, Meredith P, Burg JP. Seismicity preceding volcanic eruptions: new experimental insights. *Geology*. 2007;35:183–186. http://dx.doi.org/10.1130/G23195A.1.
15. Benson P, Vinciguerra S, Meredith P, Young R. Laboratory simulation of volcano seismicity. *Science*. 2008;322:249–252. http://dx.doi.org/10.1126/science.1161927.
16. Ito Y, Obara K, Shiomi K, Sekine S, Hirose H. Slow earthquakes coincident with episodic tremors and slow slip events. *Science*. 2007;315:503–506. http://dx.doi.org/10.1126/science.1134454.
17. Andrews I. *The Carboniferous Bowland Shale Gas Study: Geology and Resource Estimation*. British Geological Survey for Department of Energy and Climate Change: London, UK; 2003, https://www.ogauthority.co.uk/media/2782/bgs_decc_bowlandshalegasreport_main_report.pdf.
18. Sesetty V, Ghassemi A. Effect of rock anisotropy on wellbore stresses and hydraulic fracture propagation. *Int J Rock Mech Min Sci*. 2018;112:369–384. http://dx.doi.org/10.1016/j.ijrmms.2018.09.005.
19. Warpinski NR, Du J, Zimmer U. Measurements of hydraulic-fracture-induced seismicity in gas shales. *SPE*. 2012;27:240–252. http://dx.doi.org/10.2118/151597-MS.
20. Van Eijs RMHE, Mulders FMM, Nepveu M, Kenter CJ, Scheffers BC. Correlation between hydrocarbon reservoir properties and induced seismicity in the netherlands. *Eng Geol*. 2006;84:99–111. http://dx.doi.org/10.1016/j.enggeo.2006.01.002.
21. Green CA, Styles P, Baptie B. *Preese Hall Shale Gas Fracturing Review and Recommendations for Induced Seismic Mitigation Report*. Report for DECC, 2012, https://assets.publishing.service.gov.uk/government/uploads/system/uploads/attachment_data/file/48330/5055-preese-hall-shale-gas-fracturing-review-and-recomm.pdf.
22. Ellsworth WL. Injection-induced earthquakes. *Science*. 2013;341. http://dx.doi.org/10.1126/science.1225942.
23. Davies R, Foulger G, Bindley A, Styles P. Induced seismicity and hydraulic fracturing for the recovery of hydrocarbons. *Mar Pet Geol*. 2013;45:171–185. http://dx.doi.org/10.1016/j.marpetgeo.2013.03.016.
24. Clarke H, Eisner L, Styles P, Turner P. Felt seismicity associated with shale gas hydraulic fracturing: The first documented example in Europe. *Geophys Res Lett*. 2014;41:8308–8314. http://dx.doi.org/10.1002/2014GL062047.
25. Keranen KM, Weingarten M, Abers GA, Bekins BA, Ge S. Sharp increase in central oklahoma seismicity since 2008 induced by massive wastewater injection. *Science*. 2014;345(6195):448–451.
26. Zappone A, Benson PM. Effect of phase transitions on seismic properties of metapelites: new laboratory evidence. *Geology*. 2013;41:463–466. http://dx.doi.org/10.1130/G33713.1.
27. Hildreth W. Volcanological perspectives on Long Valley, Mammoth Mountain and Mono craters: several contiguous but discrete systems. *J Volcanol Geotherm Res*. 2004;136:169–1198. http://dx.doi.org/10.1016/j.jvolgeores.2004.05.019.
28. Majer EL, Baria R, Stark M, Oates S, Bommer J, Smith B, Asanuma H. Induced seismicity associated with enhanced geothermal systems. *Geothermics*. 2007;36:185–222. http://dx.doi.org/10.1016/j.geothermics.2007.03.003.
29. Häring MO, Schanz U, Ladner F, Dyer BC. Characterisation of the basel 1 enhanced geothermal system. *Geothermics*. 2008;37:469–495. http://dx.doi.org/10.1016/j.geothermics.2008.06.002.
30. Giardini D. Geothermal quake risks must be faced. *Nature*. 2009;462:848–849. http://dx.doi.org/10.1038/462848a.
31. Bachmann CE, Wiemer S, Goertz-Allmann BP, Woessner J. Influence of pore-pressure on the event-size distribution of induced earthquakes. *Geophys Res Lett*. 2012;39:L09302. http://dx.doi.org/10.1029/2012GL051480.
32. Kilburn CRJ. Fracturing as a quantitative indicator of lava flow dynamics. *J Volcanol Geotherm Res*. 2004;132(2–3):209–224. http://dx.doi.org/10.1016/S0377-0273(03)00346-9.
33. Neuberg J, Tuffen H, Collier L, Green D, Powell T, Dingwell D. The trigger mechanism of low-frequency earthquakes on montserrat. *J Volcanol Geotherm Res*. 2006;153:37–50. http://dx.doi.org/10.1016/j.jvolgeores.2005.08.008.
34. Fazio M, Benson PM, Vinciguerra S. On the generation mechanisms of fluid-driven seismic signals related to volcano tectonics. *Geophys Res Lett*. 2017;44:734–742. http://dx.doi.org/10.1002/2016GL070919.
35. Lockner DA, Walsh JB, Byerlee JD. Changes in seismic velocity and attenuation during deformation of granite. *J Geophys Res*. 1977;82:5374–5378. http://dx.doi.org/10.1029/JB082i033p05374.
36. Lockner DA, Byerlee JD. Velocity anomalies: An alternative explanation based on data from laboratory experiments. *PAGEOPH*. 1978;116:765–772. http://dx.doi.org/10.1007/BF00876537.
37. Lockner D, Byerlee J, Kuksenko V, Ponomarev A, Sidorin A. Quasi-static fault growth and shear fracture energy in granite. *Nature*. 1991;350:39–42. http://dx.doi.org/10.1038/350039a0.
38. Lei X, Kusunose K, Rao MVMSO, Satoh NT. Quasi-static fault growth and cracking in homogeneous brittle rock under triaxial compression using acoustic emission monitoring. *J Geophys Res*. 2000;105:6127–6140. http://dx.doi.org/10.1029/1999JB900385.
39. Dobson DB, Meredith PG, Boon SA. Simulation of subduction zone seismicity by dehydration of serpentine. *Science*. 2003;15:1407–1410. http://dx.doi.org/10.1126/science.1075390.
40. Thompson BD, Young RP, Lockner DA. Observations of premonitory acoustic emission and slip nucleation during a stick slip experiment in smooth faulted westerly granite. *Geophys Res Lett*. 2005;32:L10304. http://dx.doi.org/10.1029/2005GL022750.
41. Benson PM, Thompson BD, Meredith PG, Vinciguerra S, Young RP. Imaging slow failure in triaxially deformed etna basalt using 3D acoustic-emission location and X-ray computed tomography. *Geophys Res Lett*. 2007;34:L03303. http://dx.doi.org/10.1029/2006GL028721.
42. Schubnel A, Benson PM, Thompson BD, Hazard JF, Young RP. Quantifying damage, saturation and anisotropy in cracked rocks by inverting elastic wave velocities. *Pure Appl Geophys*. 2006;163:947–973. http://dx.doi.org/10.1007/s00024-006-0061-y.
43. Benson PM, Vinciguerra S, Meredith PG, Young RP. Spatio-temporal evolution of volcano seismicity: A laboratory study. *Earth Planet Sci Lett*. 2010;297:315–323. http://dx.doi.org/10.1016/j.epsl.2010.06.033.
44. Hatton CG, Main IG, Meredith PG. Non-universal scaling of fracture length and opening displacement. *Nature*. 1994;367:160–162. http://dx.doi.org/10.1038/367160a0.
45. Cowie PA, Knipe RJ, Main IG. Scaling laws for fault and fracture populations: Analyses and applications. *J Struct Geol*. 1996;18:5–11.
46. Baró J, Corral Á, Illa X, Planes A, Salje EKH, Schranz W, Soto-Parra DE, Vives E. Statistical similarity between the compression of a porous material and earthquakes. *Phys Rev Lett*. 2013;110:088702.
47. Main IG. A damage mechanics model for power-law creep and earthquake aftershock and foreshock sequences. *Geophys J Int*. 2000;142:151–161. http://dx.doi.org/10.1046/j.1365-246x.2000.00136.x.
48. Gehne S, Benson PM. Permeability and permeability anisotropy in Crab Orchard Sandstone: Experimental insights into spatio-temporal effects. *Tectonophysics*. 2017;712:589–599. http://dx.doi.org/10.1016/j.tecto.2017.06.014.
49. Goodfellow SD, Nasseri MHB, Maxwell SC, Young RP. Hydraulic fracture energy budget: Insights from the laboratory. *Geophys Res Lett*. 2015;42:3179–3187. http://dx.doi.org/10.1002/2015GL063093.
50. McLaskey GC, Lockner DA, Kilgore BD, Beeler NM. A robust calibration technique for acoustic emission systems based on momentum transfer from a ball drop. *BSSA*. 2015;105:257–271. http://dx.doi.org/10.1785/0120140170.
51. Selvadurai PA, Glaser SD. Characterizing frictional interfaces in the laboratory. *Sensors*. 2015;15:9791.

52. Brantut N, Sulem J, Schubnel A. Effect of dehydration reactions on earthquake nucleation: Stable sliding, slow transients, and unstable slip. *J Geophys Res: Solid Earth*. 2011;116(5):1–16. http://dx.doi.org/10.1029/2010JB007876.
53. Gehne S, Benson PM, Koor N, Dobson KJ, Enfield M, Barber A. Seismo-mechanical response of anisotropic rocks under simulated hydraulic fracture conditions: new experimental insights. *J Geophys Res (solid Earth)*. 2019;124. http://dx.doi.org/10.1029/2019JB017342.
54. Stoeckhert F, Molenda M, Brenne S, Alber M. Fracture propagation in sandstone and slate-laboratory experiments, acoustic emissions and fracture mechanics. *J Rock Mech Geotech Eng*. 2015;7:237–249. http://dx.doi.org/10.1016/j.jrmge.2015.03.011.
55. Browning J, Meredith PG, Stuart C, Harland S, Healy D, Mitchell TM. A directional crack damage memory effect in sandstone under true triaxial loading. *Geophys Res Lett*. 2018;45:6878–6886. http://dx.doi.org/10.1029/2018GL078207.
56. Dong J, Chen M, Li Y, Wang S, Zeng C, Zaman M. Experimental and theoretical study on dynamic hydraulic fracture. *Energies*. 2019;12:397. http://dx.doi.org/10.3390/en12030397.
57. Li N, Shicheng Z, Zou1 Y, Ma X, Zhang Z, Li1 S, Chen M, Sun Y. Acoustic emission response of laboratory hydraulic fracturing in layered shale. *Rock Mech Rock Eng*. 2018;51:3395–3406. http://dx.doi.org/10.1007/s00603-018-1547-5.
58. Lavallée Y, Benson PM, Heap MJ, Flaws A, Hess K-U, Dingwell DB. Volcanic conduit failure as a trigger to magmatic fragmentation. *Bull Volcanol*. 2011;74:11–13. http://dx.doi.org/10.1007/s00445-011-0544-2.
59. Benson PM, Lavallée Y, Heap MJ, Flaws A, Hess KU, Dingwell DB. Laboratory simulations of tensile fracture via cyclical magma pressurisation. *Earth Planet Sci Lett*. 2012;349:231–239. http://dx.doi.org/10.1016/j.epsl.2012.07.003.
60. Lister JR, Kerr RC. Fluid-mechanical models of crack propagation and their application to magma-transport in dykes. *J Geophys Res*. 1991;96:10049–10077. http://dx.doi.org/10.1029/91JB00600.
61. Taisne B, Tait S. Effect of solidification on a propagating dike. *J Geophys Res*. 2011;116:B01206. http://dx.doi.org/10.1029/2009JB007058.
62. Bakker R, Fazio M, Benson PM, Hess KU, Dingwell DB. The propagation and seismicity of dyke injection, new experimental evidence. *Geophys Res Lett*. 2016;43:1876–1883. http://dx.doi.org/10.1002/2015GL066852.
63. Tuffen H, Dingwell DB, Pinkerton H. Repeated fracture and healing of silicic magma generate flow banding and earthquakes?. *Geology*. 2003;31:1089–1092. http://dx.doi.org/10.1130/G19777.1.
64. Rocchi V, Sammonds PR, Kilburn CRJ. Fracturing of etnean and vesuvian rocks at high temperatures and low pressures. *J Volcanol Geotherm Res*. 2004;132:137–157. http://dx.doi.org/10.1016/S0377-0273(03)00342-1.
65. Smith R, Sammonds PR, Kilburn CRJ. Fracturing of volcanic systems: experimental insights into pre-eruptive conditions. *Earth Planet Sci Lett*. 2009;280:211–219. http://dx.doi.org/10.1016/j.epsl.2009.01.032.
66. Chandler MR, Meredith PG, Brantut N, Crawford BR. Fracture toughness anisotropy in shale. *J Geophys Res: Solid Earth*. 2016;121:1706–1729. http://dx.doi.org/10.1002/2015JB012756.
67. Vinciguerra S, Meredith PG, Hazzard J. Experimental and modeling study of fluid pressure-driven fractures in Darley Dale sandstone. *Geophys Res Lett*. 2004;31:L09609. http://dx.doi.org/10.1029/2004GL019638.
68. Stanchits S, Mayr S, Shapiro S, Dresen G. Fracturing of porous rock induced by fluid injection. *Tectonophysics*. 2011;503:129–145. http://dx.doi.org/10.1016/j.tecto.2010.09.022.
69. Fazio M, Alparone S, Benson PM, Cannata A, Vinciguerra S. Genesis and mechanisms controlling Tornillo seismo-volcanic events in volcanic areas. *Nat Sci Rep*. 2019;9:7338. http://dx.doi.org/10.1038/s41598-019-43842-y.
70. Zoback M, Rummel F, Jung R, Raleigh C. Laboratory hydraulic fracturing experiments in intact and pre-fractured rock. *Int J Rock Mech Min Sci Geomech Abstr*. 1977;14:49–58. http://dx.doi.org/10.1016/0148-9062(77)90196-6.
71. Schmitt DR, Zoback M. Diminished pore pressure in low-porosity crystalline rock under tensional failure; apparent strengthening by dilatancy. *J Geophys Res Atmos*. 1992;97:273–288. http://dx.doi.org/10.1029/91JB02256.
72. Rummel F, Hansen J. Interpretation of hydrofrac pressure recordings using a simple fracture mechanics simulation model. *Int J Rock Mech Min Sci Geomech Abstr*. 1989;26:483–488. http://dx.doi.org/10.1016/0148-9062(89)91425-3.
73. Zang A, Zimmermann G, Hofmann H, Stephansson O, Min K-B, Kim K-Y. How to reduce fluid-injection-induced seismicity. *Rock Mech Rock Eng*. 2019;52:475–493. http://dx.doi.org/10.1007/s00603-018-1467-4.
74. Gehne S, Benson PM. Permeability enhancement through hydraulic fracturing: new laboratory measurements combining a 3D printed jacket and direct over-pressure. *Nat Sci Rep*. 2019;9:12573. http://dx.doi.org/10.1038/s41598-019-49093-1.
75. Burlini L, Di Toro G, Meredith P. Seismic tremor in subduction zones: Rock physics evidence. *Geophys Res Lett*. 2009;36:8305. http://dx.doi.org/10.1029/2009GL037735.
76. Brantut N, Schubnel A, David EC, Heripre E, Guéguen Y, Dimanov A. Dehydration-induced damage and deformation in gypsum and implications for subduction zone processes. *J Geophys Res*. 2012;117:B03205. http://dx.doi.org/10.1029/2011JB008730.
77. Bakker R, Violay ES, Benson PM, Vinciguerra SV. Ductile flow in subvolcanic carbonate basement as the main control for edifice stability: new experimental insights. *Earth Planet Sci Lett*. 2015;430. http://dx.doi.org/10.1016/j.epsl.2015.08.017, 553-541.
78. Birch F. The velocity of compressional waves in rocks to 10 kilobars: 1. *J Geophys Res*. 1960;65:1083–1102. http://dx.doi.org/10.1029/JZ065i004p01083.
79. Goebel THW, Becker TW, Schorlemmer D, Stanchits S, Sammis C, Rybacki E, Dresen G. Identifying fault heterogeneity through mapping spatial anomalies in acoustic emission statistics. *J Geophys Res*. 2012;117:B03310. http://dx.doi.org/10.1029/2011JB008763.
80. Thompson BD, Young RP, Lockner DA. Fracture in westerly granite under AE feedback and constant strain rate loading: Nucleation, quasi-static propagation, and the transition to unstable fracture propagation. *Pure Appl Geophys*. 2006;163:995–1019.
81. Benson PM, Meredith PG, Schubnel A. Role of void space geometry in permeability evolution in crustal rocks at elevated pressure. *J Geophys Res: Solid Earth*. 2006;111:B12203. http://dx.doi.org/10.1029/2006JB004309.
82. King T, Benson PM, De Siena L, Vinciguerra S. Investigating the apparent seismic diffusivity of near-receiver geology at Mount St. Helens Volcano, USA. *Geosciences*. 2018;7:130. http://dx.doi.org/10.3390/geosciences7040130.
83. Nasseri MHB, Benson PM, A. Schubnel, Young RP. Common evolution of mechanical and transport properties in thermally cracked westerly granite at elevated hydrostatic pressure. *Pure Appl Geophys*. 2009;166:927–948. http://dx.doi.org/10.1007/s00024-009-0485-2.
84. Colombero C, Comina C, Vinciguerra S, Benson PM. Microseismicity of an unstable rock mass: From field monitoring to laboratory testing. *J Geophys Res: Solid Earth*. 2018;123:1673–1693. http://dx.doi.org/10.1002/2017JB014612.
85. Audet P, Bostock MG, Christen NI, Peacock SM. Seismic evidence for overpressured subducted oceanic crust and megathrust fault sealing. *Nature*. 2009;457:76–78. http://dx.doi.org/10.1038/nature07650.
86. Vinciguerra S, Trovato C, Meredith P, Benson PM. Relating seismic velocities, thermal cracking and permeability in Mt. Etna and Iceland basalts. *Int J Rock Mech Min Sci*. 2005;42:900–910. http://dx.doi.org/10.1016/j.ijrmms.2005.05.022.
87. Vinciguerra S, Trovato C, Meredith P, Benson PM, De Luca G, Troise C, De Natale G. The seismic velocity structure of Campi flegrei caldera (Italy): from the laboratory to the field scale. *Pure Appl Geophys*. 2006;163:2205–2221. http://dx.doi.org/10.1007/s00024-006-0118.
88. Browning J, Meredith P, Gudmundsson A. Cooling-dominated cracking in thermally stressed volcanic rocks. *Geophys Res Lett*. 2016;43:8417–8425. http://dx.doi.org/10.1002/2016GL070532.
89. Harnett CE, Benson PM, Rowley P, Fazio M. Fracture and damage localization in volcanic edifice rocks from El Hierro, Stromboli and Tenerife. *Nat Sci Rep*. 2018;8:1942. http://dx.doi.org/10.1038/s41598-018-20442-w.
90. Castagna A, Ougier-Simonin A, Benson PM, Browning J, Walker RJ, Fazio M, Vinciguerra S. Temperature and pore pressure effects on brittle-ductile transition of comiso limestone. *J Geophys Res*. 2018;123:7644–7660. http://dx.doi.org/10.1029/2017JB015105.
91. Ayling MR, Meredith PG, Murrell SAF. Microcracking during triaxial deformation of porous rocks monitored by changes in rock physical properties. I. Elastic-wave propagation measurements on dry rocks. *Tectonophysics*. 1995;245:205–221. http://dx.doi.org/10.1016/0040-1951(94)00235-2.
92. De Natale G, Troise C, Trigila R, Dolfi D, Chiarabba C. Seismicity and 3-D substructure at somma-vesuvius volcano: evidence for magma quenching. *Earth Planet Sci Lett*. 2004;221:181–196. http://dx.doi.org/10.1016/S0012-821X(04)00093-7.
93. De Natale G, Troise C, Mark D, Mormone A, Piochi M, Di Vito MA, Isaia R, Carlino S, Barra D, Somma R. The Campi Flegrei Deep Drilling Project (CFDDP): New insight on caldera structure, evolution and hazard implications for the Naples area (Southern Italy). *Geochem Geophys Geosyst*. 2016;17:4836–4847. http://dx.doi.org/10.1002/2015GC006183.
94. Scholz CH. *The Mechanics of Earthquakes and Faulting*. 2nd ed., Cambridge Univ. Press: Cambridge, UK; 2002.
95. Chouet BA, Page RA, Stephens CD, Lahr JC, Power JAJ. Precursory swarms of long-period events at Redoubt Volcano (1989 1990). Alaska: Their origin and use as a forecasting tool. *J Volcanol Geotherm Res*. 1994;62:95–135. http://dx.doi.org/10.1016/0377-0273(94)90030-2.
96. Rogers G, Dragert H. Episodic tremor and slip on the Cascadia subduction zone: The chatter of silent slip. *Science*. 2003;300:1942–1943. http://dx.doi.org/10.1126/science.1084783.
97. Rubinstein J, Vidale JE, Gomberg J, Bodin P, Creager KC, Malone SD. Non-volcanic tremor driven by large transient shear stresses. *Nature*. 2007;448:579–582. http://dx.doi.org/10.1038/nature06017.

98. Julian BR. Volcanic tremor: Non-linear excitation by fluid flow. *J Geophys Res*. 1994;99:11859–11877. http://dx.doi.org/10.1029/93JB03129.
99. Torres RA, Gomez DM, Narvaez ML. Unusual seismic signals associated with the activity at galeras volcano, Colombia, from 1992 to 1994. *Ann Geophys*. 1996;39:299–310.
100. Gómez MDM, Torres C, Roberto A. Unusual low-frequency volcanic seismic events with slowly decaying coda waves observed at galeras and other volcanoes. *J Volcanol Geotherm Res*. 1997;77:173–193. http://dx.doi.org/10.1016/S0377-0273(96)00093-5.
101. Lavallée Y, Benson PM, Heap MJ, Hess K-U, Flaws A, Schillinger B, Meredith PG, Dingwell DB. Reconstructing magma failure and the degassing network of dome-building eruptions. *Geology*. 2013;41:515–518. http://dx.doi.org/10.1130/G33948.1.
102. Benson P, Meredith P, Platzman E, White R. Pore fabric shape anisotropy in porous sandstones and its relation to elastic wave velocity and permeability anisotropy under hydrostatic pressure. *Int J Rock Mech Min Sci*. 2005;42:890–899. http://dx.doi.org/10.1016/j.ijrmms.2005.05.003.
103. Gandossi L. *An Overview of Hydraulic Fracturing and Other Formation Stimulation Technologies for Shale Gas Production*. Eur. Commission Jt. Res. Cent. Tech. Reports, 2013, http://dx.doi.org/10.2790/133987.
104. Heap MJ, Vinciguerra S, Meredith PG. The evolution of elastic moduli with increasing crack damage during cyclic stressing of a basalt from Mt. Etna volcano. *Tectonophysics*. 2009;471:153–160. http://dx.doi.org/10.1016/j.tecto.2008.10.004.
105. O'Toole T, Verdon JP, Woodhouse JH, Kendall JM. Induced seismicity at Preese Hall, UK—A review. In: *75th EAGE Conference and Exhibition incorporating SPE EUROPEC 2013*, London, 2013.
106. Bell AF, Naylor M, Heap MJ, I.G. Main. Forecasting volcanic eruptions and other material failure phenomena: An evaluation of the failure forecast method. *Geophys Res Lett*. 2011;38:L15304. http://dx.doi.org/10.1029/2011GL048155.
107. Bean CJ, De Barros L, Lokmer I, Metaxian J, O'Brien G, Murphy S. Long-period seismicity in the shallow volcanic edifice. *Nat Geosci*. 2014;7:71–75. http://dx.doi.org/10.1038/ngeo2027.
108. Kilburn CRJ, De Natale G, Carlino S. Progressive approach to eruption at Campi flegrei caldera in southern Italy. *Nature Commun*. 2017;8:15312. http://dx.doi.org/10.1038/ncomms15312.
109. Benson PM, Vinciguerra S, Nasseri MHB, Young RP. Laboratory simulations of fluid/gas induced micro-earthquakes: application to volcano seismology. *Front Earth Sci*. 2014;2:32. http://dx.doi.org/10.3389/feart.2014.00032.